Evolution of the Eutectic Microstructure in Chemically Modified and Unmodified Aluminum Silicon Alloys

by

Hema V. Guthy

A Thesis

Submitted to the Faculty

of the

WORCESTER POLYTECHNIC INSTITUTE

in partial fulfillment of the requirements for the

Degree of **Master of Science**

in

Materials Science and Engineering

April 2002

APPROVED:

_____

Prof. Makhlouf. M. Makhlouf, Major Advisor

_____

Prof. Richard D. Sisson, Jr Materials Science and Engineering Group Head

ABSTRACT

Aluminum-silicon alloys are an important class of commercial non-ferrous alloys having wide ranging applications in the automotive and aerospace industries. Typical aluminum-silicon alloys have two major microstructural components, namely primary aluminum and an aluminum-silicon eutectic. While nucleation and growth of the primary aluminum in the form of dendrites have been well understood, the understanding of the evolution of the Al-Si eutectic is still incomplete. The microstructural changes caused by the addition of strontium to these alloys are another important phenomenon that still puzzles the scientific community. In this thesis, an effort has been made to understand the evolution of the Al-Si eutectic in the presence and absence of strontium through two sets of experiments: (1) Quench experiments, and (2) sessile drop experiments. The quench experiments were designed to freeze the evolution of the eutectic after various time intervals along the eutectic plateau. The sessile drop experiments were designed to study the role of surface energy in the formation of the eutectic in the presence and absence of strontium. Both experiments were conducted on high purity alloys. Using observations from these experiments, possible mechanism(s) for the evolution of the Al-Si eutectic and the effects of strontium on modifying the eutectic morphology are proposed.

ACKNOWLEDGEMENTS

I am deeply indebted to Prof. M. M. Makhlouf for giving me an opportunity to work with him on this project. His words of encouragement and motivation came a long way in bringing this work to fruition. Prof. D. Apelian's advice and guidance throughout this work has been of immeasurable help not only in academic work, but also in my development as a whole. I would also like to thank Prof. R. R. Biederman for his continual input and help in microstructural analysis. I would also like to thank my colleagues Deepak, Olivier, Manas, Nasim, Libo and Diana for helping me in my work. I want to take this opportunity to thank the staff of Metals Processing Institute and the department of Materials science and Engineering for providing a conducive and friendly atmosphere. Last but not the least, I am deeply indebted to Dr. Sumanth Shankar for his interest and support in doing this work. Without his help, this project would not have been even half as much interesting or fun as it has been.

TABLE OF CONTENTS

LIST OF TABLES

LIST OF FIGURES

1. INTRODUCTION

Aluminum-Silicon alloys constitute a important class of aluminum foundry alloys. Aluminum alloys with silicon as major alloying element offer excellent castability, good corrosion resistance and can be easily welded and machined. Sand and permanent mold cast binary aluminum silicon alloys are used in many automotive, domestic food and pump castings. Premium quality castings are used in military and aircraft applications.

Aluminum silicon foundry alloys are usually alloyed close to the eutectic or near eutectic compositions due to the small freezing range, good castability and desirable properties obtained at these compositions. The most important aluminum silicon alloys are based on the aluminum-silicon system, especially the hypoeutectic alloys with compositions ranging from 7 to 11 wt. % silicon.

Understanding the mechanism by which the eutectic forms and grows is important. During the solidification of aluminum silicon alloys, first the primary dendrites grow. After the dendrites impinge upon each other, the dendrite mobility is restricted. Mass transport to compensate for shrinkage occurs mainly by interdendritic feeding. Interdendritic feeding involves the flow of eutectic liquid. Thus, the origin and growth of the eutectic is of major importance to fluid flow.

Hence, the understanding of mechanism of eutectic formation helps in analyzing the resistance to melt flow and the feeding efficiency. These further affect the shrinkage, porosity formation and segregation.

Further, Aluminum-silicon eutectic is an anomalous eutectic because it constitutes a metal (aluminum) and a non-metal (silicon). Evolution of an anomalous eutectic has not been completely understood till date. To add to the confusion, the aluminum-silicon eutectic undergoes a change in morphology upon addition of certain elements e.g. strontium or sodium. This process is often referred to as eutectic modification. The exact mechanism of modification is still not well understood despite of decades of research.

In this work an effort has been made to further our understanding of the formation of the aluminum silicon eutectic both in unmodified and modified alloys and applying our understanding to alleviate the problems of porosity in castings.

The work is organized into different sections: *Background*, reviews the literature available till date on eutectic evolution; *Design of experiments and Procedures*, details the plan, materials and procedures used in conducting the various experiments; *Results and Discussion*, describes the results obtained and corelates it with the understanding available from the literature.

2. BACKGROUND

In this section, a review of the basics of aluminum silicon system and the present understanding of the evolution of aluminum silicon eutectic in hypoeutectic alloys is presented. After a brief discourse on the equilibrium cooling behavior of aluminum-silicon alloys, the remainder of this section discusses the mechanisms of nucleation and growth of silicon. In section 2.2, the evolution of different microstructures of pure aluminum silicon eutectic (without chemical modifiers) at different parameters is discussed. The evolution of chemically modified microstructure of the eutectic is dealt with in section 2.3. The changes associated with the process of modification are discussed in section 2.3.1 and sections 2.3.2 discuss the various theories in the literature trying to explain the observations.

2.1 The Aluminum-Silicon Phase Diagram and Equilibrium Cooling

Aluminum-Silicon system is a simple binary eutectic with limited solubility of aluminum in silicon and limited solubility of silicon in aluminum. The solubility of silicon in aluminum reaches a maximum 1.5 at% at the eutectic temperature, and the solubility of silicon increases with temperature to 0.016% Si at 1190°C. Figure 1 depicts the contemporary aluminum-silicon phase diagram. There is only one invariant reaction in this diagram, namely

$$L \rightarrow \alpha + \beta \quad \text{(eutectic)} \tag{1}$$

In equation (1), L is the liquid phase, α is predominantly aluminum, and β is predominantly silicon. It is now widely accepted that the eutectic reaction takes place at 577°C and at a silicon level of 12.6%[1]. Figure 1 shows that the aluminum-silicon eutectic can form as follows:

1. Directly from the liquid in the case of a silicon concentration of 12.6% (i.e., for a eutectic aluminum-silicon alloy),
2. In the presence of primary aluminum in the case of silicon contents <12.6% (i.e., for hypoeutectic aluminum-silicon alloys), and
3. In the presence of primary silicon crystals in the case of silicon contents >12.6% (for hypereutectic aluminum-silicon alloys).

Typical eutectic structures of binary alloys form by the simultaneous growth of two phases from the liquid; therefore they may exhibit a variety of microstructures that can be classified according to two criteria:

- Lamellar vs. fibrous morphology of the individual phases, and
- Regular vs. irregular growth of the individual phases.

[1] Unless otherwise stated, all compositions are in wt.%.

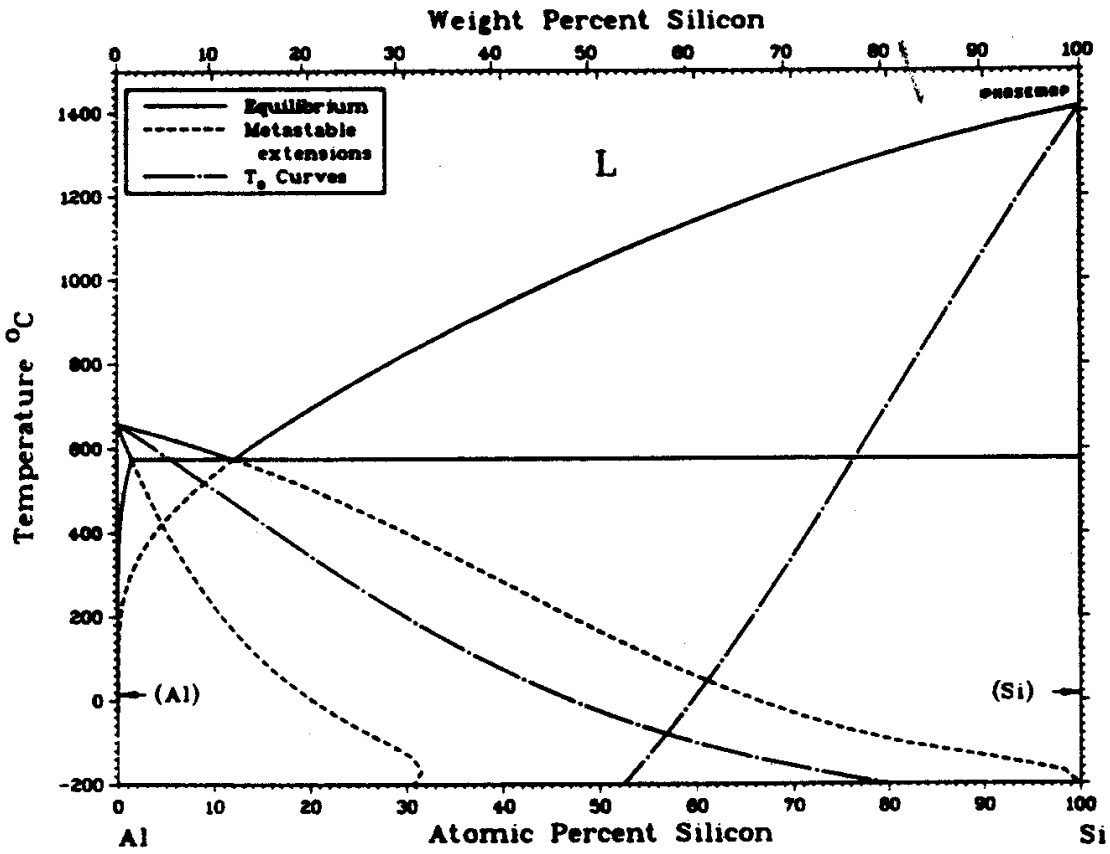

Figure 1: Equilibrium diagram for the Al-Si system showing metastable extensions of liquidus and solidus lines [1]

Figure 2 shows the microstructure of the aluminum-silicon eutectic. In general, when there are approximately equal volume fractions of the two phases, eutectics of binary alloys exhibit a lamellar structure. On the other hand, if one phase is present in a small volume fraction, this phase tends to be fibrous. As a rule of thumb, the eutectic microstructure obtained will tend to be fibrous when the volume fraction of the minor phase is less than 0.25, otherwise it will tend to be lamellar. [2] If both phases in the eutectic are non-faceted, the eutectic will exhibit a regular morphology. In this case, the microstructure is made up of

either lamellae or fibers having a high degree of regularity and periodicity. On the other hand, if one phase is faceted, the eutectic morphology is often irregular. Even though the volume fraction of silicon in the aluminum-silicon binary is less than 0.25[2], the typical aluminum-silicon eutectic is closer to a lamellar structure than to a fibrous one. This is usually attributed to the strong anisotropy of growth of silicon and to the relatively low interfacial energy between silicon and aluminum. [2]

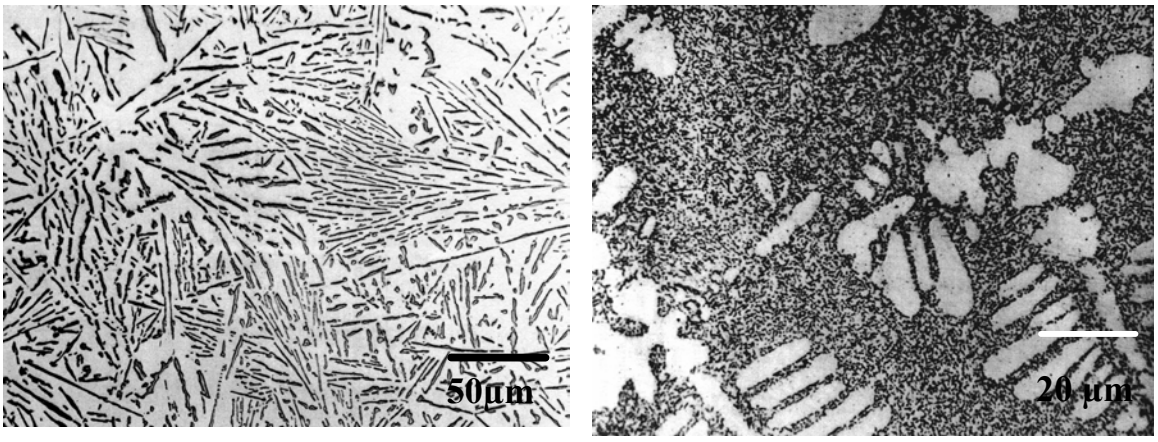

Figure 2: Al-12.5wt% Si alloy (a) Slowly cooled 200X (b) Chill Cast 500X [3]

Gwyer and Phillips [4] determined the composition and temperature of the eutectic reaction in the Al-Si binary system to be 11.7%Si and 577°C respectively. Though the eutectic temperature is in accord with the currently accepted value, the eutectic composition was later changed to 12.2 ± 0.1 atom %Si. [5, 6] The initial error in establishing the eutectic point is due to the fact that the temperature of formation of the primary constituents (aluminum and silicon), as well as the temperature of the Al-Si eutectic plateau are cooling rate

[2] The volume fraction of silicon in an Al-Si eutectic is 0.143.

dependent. Primary silicon undercools more than primary aluminum hence the eutectic structure forms at 10-12°C below the eutectic temperature without appreciable recalescence. [7] Consequently, at higher cooling rates, the system behaves as though the eutectic point is shifted to higher silicon contents and the eutectic temperature is depressed. Figure 2 illustrates this apparent shift in the eutectic point. Figure 2(a), which depicts the microstructure of a eutectic aluminum-silicon alloy that is slowly cooled, shows no primary aluminum; on the other hand, Figure 2(b), which depicts the microstructure of the same alloy cooled at a relatively faster rate, shows primary aluminum dendrites.

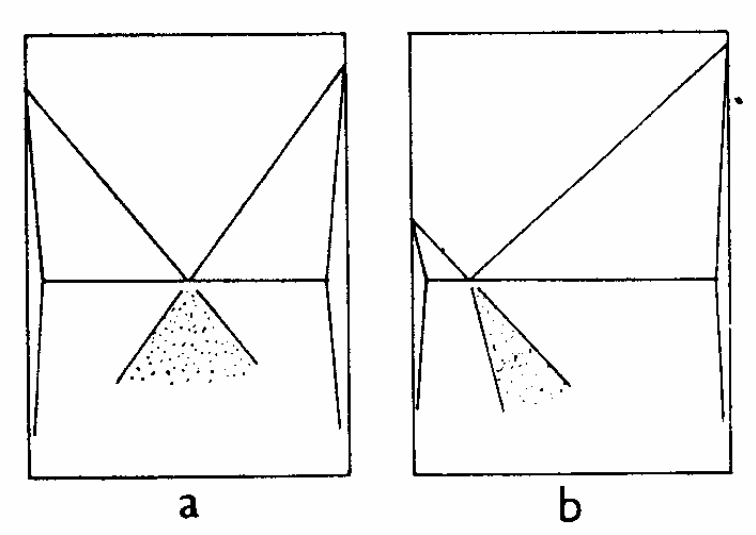

Figure 3: Coupled zone in (a) symmetrical and (b) asymmetrical Phase diagrams [3]

Depression of the eutectic temperature with increased cooling rate may be explained on the basis of the coupled region effect. [8, 9] Coupled regions represent fields within the phase diagram where the two phases of the eutectic

are organized in the solid in such a way as to allow diffusion in the liquid to occur effectively at a duplex solid/liquid front. [6, 8, 10-12] Regions of coupled growth are shown schematically in Figure 3 for both a symmetric and an asymmetric hypothetical phase diagram. In Al-Si system, silicon is a non-metal, which has directed covalent bonding. Hence silicon phase tends to grow anisotropically to give faceted crystals. Silicon phase needs more under-cooling for its growth than the isotropic aluminum phase. Thus the coupled region in such a system is asymmetric. Apart from cooling rate, addition of some chemical elements like sodium or strontium in minute quantities resulted in shifting the eutectic point to the right as well as depressing the eutectic temperature. The reason for the same are discussed in following sub-sections. As science of solidification progressed, cooling rate was replaced with two independent parameters which determined the phase diagram and resulting microstructure: Temperature gradient (G) and Interface velocity (R). The importance and the effect of G and R are discussed in section 2.2.

2.2 Unmodified Alloy

In this sub-section, the various microstructures of pure aluminum silicon alloy both hypoeutectic and hypereutectic are presented. The various silicon morphologies obtained at different interface velocities and temperature gradients are shown and their possible growth mechanisms discussed.

During the solidification of metals, the melt conditions determine the morphology of the solidifying phase. Melt conditions include both thermal conditions and

chemical conditions. Thermal conditions during solidification consist of three parameters: cooling rate, thermal gradient (G) and interface velocity (R). Cooling rate is the rate at which heat (or temperature) is extracted from the melt. Higher cooling rate is known to yield finer structures. The cooling rate is inversely related to the secondary dendrite arm spacing. Thermal gradient (G) is the change of temperature with distance. Thermal gradient of liquid ahead of the solid/liquid interface determines the constitutional under-cooling of the liquid. Constitutional under-cooling is known to result in cellular and dendritic morphology. [13] Interface velocity (R) is the rate at which the solid/liquid interface moves. High interface velocity implies lesser time for equilibrium growth to take place. Thus, microstructures obtained at higher interface velocities have finer structure and sometimes metastable structures. Cooling rate is the product of thermal gradient and interface velocity. Comprehensive study of the different microstructures possible in a system is done by studying the system at various values of temperature gradient and interface velocity. In the following section, the various possible microstructures of aluminum-silicon eutectic and primary silicon in hypereutectic alloys and their possible growth mechanisms are discussed.

2.2.1 Various Silicon Microstructures and their Growth Mechanisms

In this section the different silicon microstructures of aluminum silicon eutectic and primary silicon at varying temperature gradients and interface velocities are discussed.

Day and Hellawell [14] conducted a detailed study to identify the different forms of silicon in the aluminum-silicon eutectic as a function of the temperature gradient (G), the growth rate (V) and alloy chemistry. They classified the microstructures of directionally solidified Al-Si eutectic alloys into four distinct forms corresponding to the regions marked as A, B, C, and D in Figure 4. The different microstructures and the possible growth mechanisms are discussed henceforth.

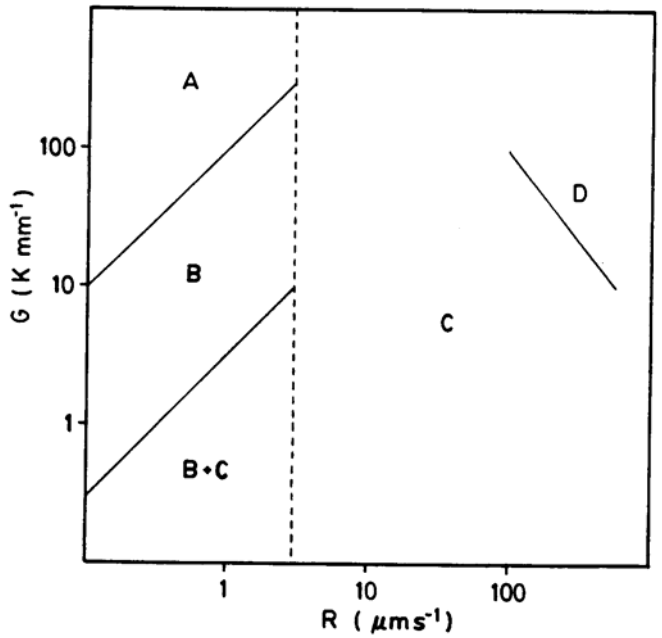

Figure 4: Different regions of silicon morphology as a function of Growth rate and solidification rate [14]

Region A

The microstructure in region A is characterized by massive silicon particles growing by long-range diffusion. The solidification interface is essentially planar

and isothermal. Some of the silicon crystals are interconnected, and the individual silicon crystals are irregular, banded, and tend to contain numerous {111}-growth twins. [14] However other studies [15] have shown that silicon grows in the form of platelets by TPRE growth mechanism.(to be discussed in the section on Region C). It is believed that [16] the high value of the G/V ratio ($>10^{7}$°C s cm^{-2}) prevents constitutional under-cooling of the aluminum phase by the silicon phase and hence the aluminum phase grows with a planar interface. Quenched structures of directionally solidified samples reveal that silicon leads at the interface, [15] while growing in a very faceted manner. However at some regions silicon and aluminum were found to be growing together. In such cases the silicon phase in contact with the aluminum was distinctly non-faceted.

Figure 5: Longitudinal section of a sample from region A [14]

Region B

In the region marked B, silicon assumes a variety of morphologies depending on the temperature gradient (G). At higher temperature gradients, close to those of

the region marked A, silicon appears as fibers with a round cross-section as shown in Figure 6. But as the temperature gradient decreases, the silicon forms lateral branches with a characteristic four-fold symmetry as shown in Figure 7. [17-19] According to Bell and Winegard, [18] the higher partition coefficient of silicon in aluminum (0.14), causes a higher buildup of aluminum ahead of the silicon phase than the buildup of silicon ahead of the aluminum phase. Thus the liquid ahead of the silicon phase becomes constitutionally more undercooled favoring growth along definite crystallographic directions; typically, the [100] direction. Hellawell [3,14] views the transition from the region marked A to that marked B as equivalent to single phase planar to cellular transformation with the silicon nucleating in the intercellular nodes of aluminum. Elliott [16] observed that for relatively low G/V ratios, radial and lateral solute diffusion accompanying the formation of the silicon phase lead to reduced solute accumulation ahead of the solid/liquid interface thus giving the silicon phase a lead over the aluminum phase during solidification. As the G/V ratio decreases further, the lead of the silicon phase over the aluminum phase increases making it conducive for silicon particles to grow in between the angular silicon. [17,19] The new silicon particles appearing in between the angular silicon phase display a flake-like morphology and are interconnected. The flaky silicon is the predominant form in region C.

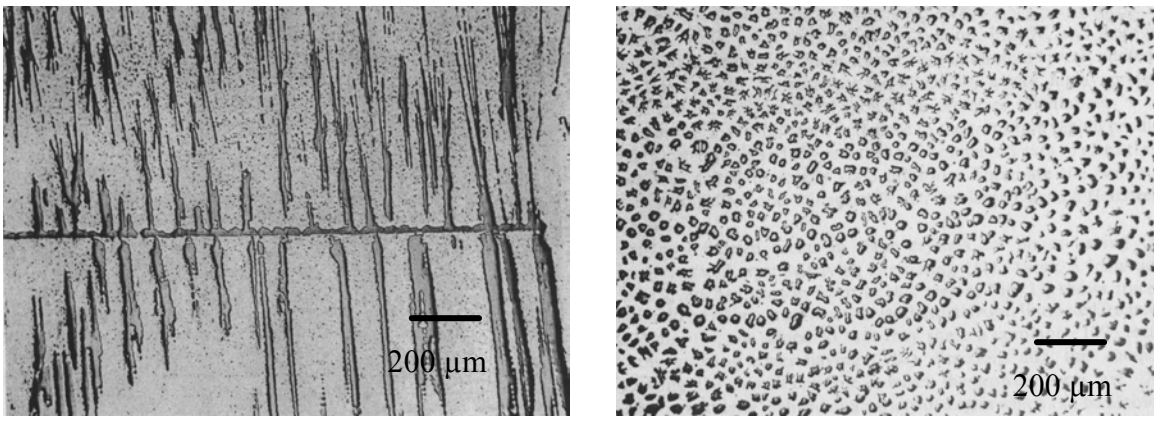

Figure 6: (a) Longitudinal section of sample from region B (b) Transverse section of sample from region B [14]

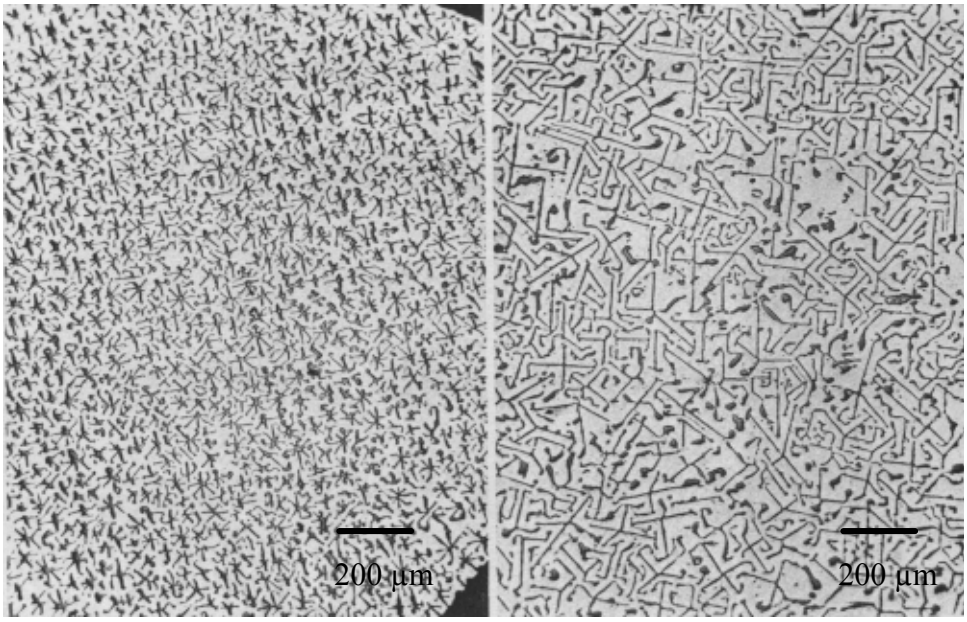

Figure 7: Microstructures of directionally solidified Al-Si eutectic alloy in region B with a interface velocity of 0.28 μm/s and with temperature gradient of (a) 12 ºC/mm (b) 3 ºC/mm [14]

Region C

The flaky silicon which appears in between the angular silicon in region B + C, starts predominating when the interface velocity is increased.(refer Figure 4) The flaky silicon is the general class of irregular eutectic observed in unmodified alloys. All commercial castings solidify in this regime of interface velocity (R) and temperature gradient (G). The silicon exists in the form of flakes, but in the two dimensional microstructures it appears as rods as shown in Figure 2. It is very important to understand the growth mechanism of flaky silicon because of its relevance to the phenomenon of modification. Most of the theories which explain modification assume a change in growth mechanism of silicon. So unless a complete understanding of growth of flaky silicon is available, theories of modification would still be incomplete. However, the exact growth mechanism of flaky silicon is still under debate. The various possible growth mechanisms in flaky silicon are discussed henceforth.

Twin Plane Re-entrant edge (TPRE) Mechanism

The TPRE mechanism was first introduced by Hamilton and Seindensticker [20] to explain the growth of germanium dendrites and was later extended to the growth of silicon. The equilibrium habit of silicon is an octahedron bound by eight {111} planes. A twin crystal is half of the equilibrium crystal reflected across the remaining solid along the twin composition plane. Consequently, the outline of the twin silicon crystal consists of six edges of the intersection of pairs of {111} planes as shown in Figure 8(a). The external angles between these

bounding planes are 141° and 219°. The bounding planes that make a 141° external angle form a re-entrant corner, while those planes that make a 219° external angle form a ridge. Because of the more favorable bonding for an atom joining a re-entrant corner than one joining a ridge, re-entrant corners are more favorable nucleation sites than ridges.

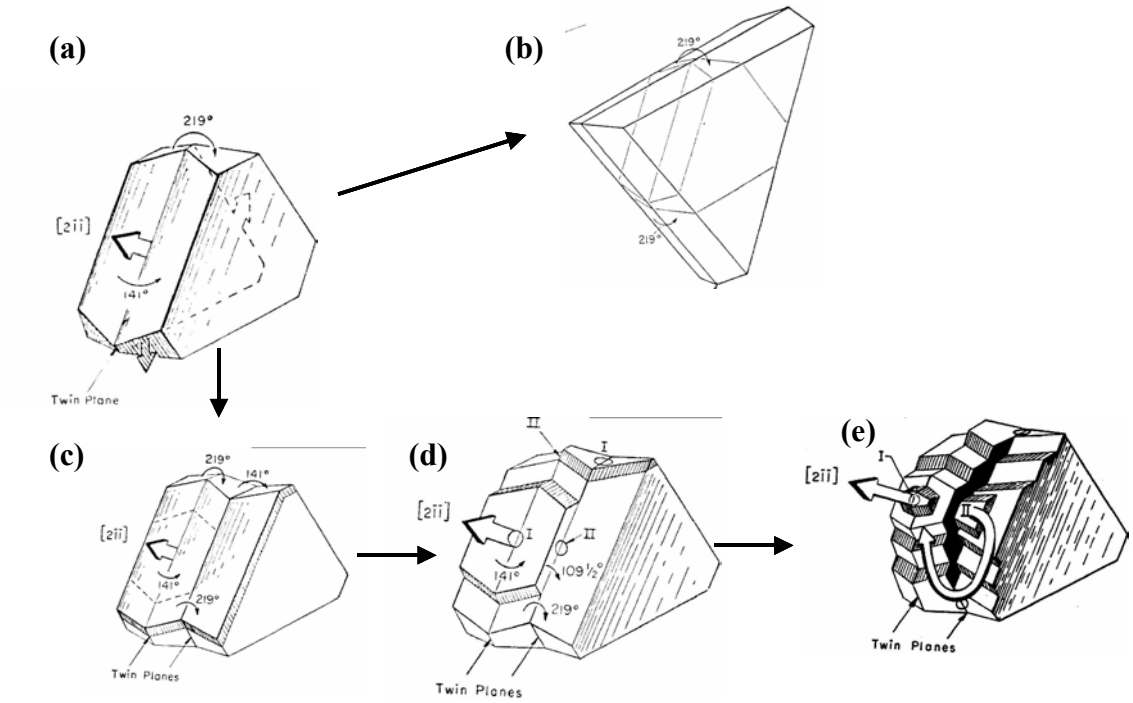

Figure 8: Twin Plane Reentrant Edge Mechanism (a) Crystal with a single twin (b) Closure of twins due to ridge formation (c) Crystal with two twins (d) Creation of extra reentrant corners I and II (e) Propagation of crystal due to reentrant corners [20]

Thus, the presence of a re-entrant corner leads to rapid growth along the [211] direction. However, this rapid growth on the re-entrant corner stops when a

trigonal solid that is bounded entirely by ridges is formed (Figure 8(b)). However, if the crystal has two twins instead of one as shown in Figure 8(c), it will have six re-entrant corners located along the <211> direction. Growth on the re-entrant corners now generates more re-entrant corners as shown in Figure 8(d) and the newly generated re-entrant corners relieve the blockage of nucleation sites that is caused by the formation of ridges. Figure 8(e) shows a solid with several steps that are growing simultaneously by the re-entrant edge mechanism. Billig and Holmes [21] experimentally verified that the TPRE mechanism is responsible for the growth of germanium dendrites and observed that all germanium dendrites invariably contain two or more twins and never a single twin. However, it has not been experimentally verified that the TPRE mechanism is the mechanism responsible for the growth of silicon dendrites or flake-like silicon.

Layer Growth Mechanism

Materials with high entropy of melting like silicon tend to form atomically smooth, close packed interfaces. [13] Thus any atom leaving the liquid and attaching itself to flat solid surface increases the interfacial energy. Thus, the atom is likely to jump back into the liquid. However, if the interface contains ledges, liquid atoms will be easily able to join the solid without increasing the interfacial energy as shown in Figure 9.

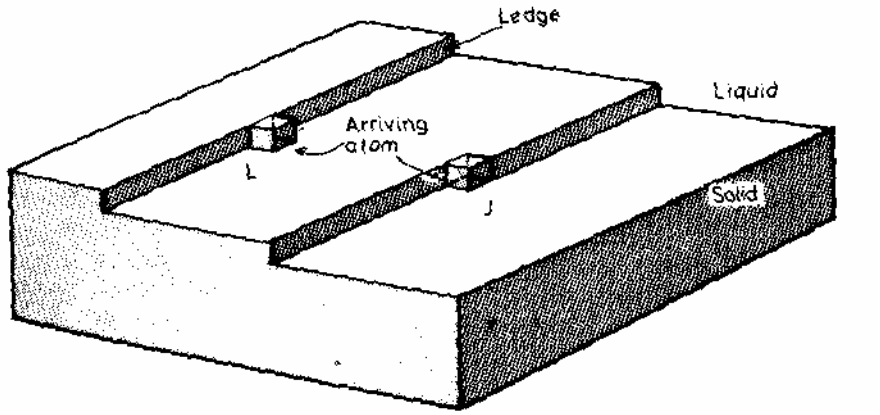

Figure 9: Layer growth mechanism of atomically smooth interfaces by formation of ledges [13]

Hellawell et al [22,23] suggested that silicon in the flake form grows predominantly by layer growth mechanism. The authors measured the average twin spacing of twins to be about 0.4 to 1.0μm in slowly cooled specimens. They observed that twin spacing are much wider than that would be expected from TPRE mechanism. Moreover, microstructural analysis using TEM revealed that twins emerge on the non faceted part of silicon crystal and does not form any re-entrant edges or grooves. However, no conclusive evidence of the operation of layer mechanism was presented. On this premise, a theory explaining the modification phenomenon was proposed, which will be discussed in section 2.3.2.

Screw Dislocations

Though layer growth mechanism explains how growth proceeds once the ledges are formed, the nucleation of layers are very important and need to be understood. One of the sources for nucleation of new layers is screw

dislocations. Crystallographers have studied the effect of screw dislocations in nucleating new layers and its interactions with re-entrant edges. A brief overview of literature available from crystal growth studies on the role of screw dislocation in the growth of faceted crystals is presented.

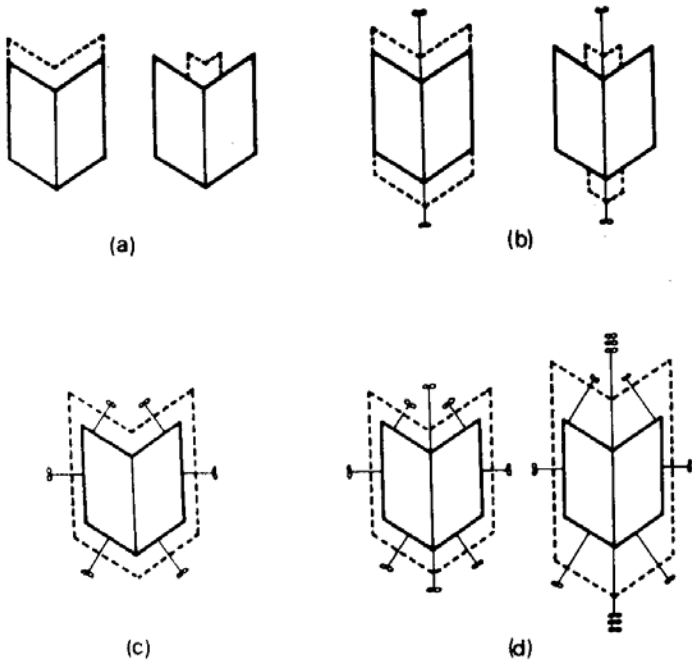

Figure 10: Hypothetical Cases of screw dislocation and reentrant corner effect [24]

Kitamura et al [24] questioned the adoption of the TPRE mechanism to explain growth in real crystals because it was originally developed for perfect crystals. [25] Kitamura et al argue that screw dislocations, which are prevalent in real crystals, should be accounted for when developing a growth mechanism for faceted crystals. Hence, they considered four different cases based on the presence or absence of screw dislocations and twin junctions on the surface of a

crystal as shown in Figure 10. There are basically four preferential growth sites in a given faceted crystal. Listed in decreasing order of their effectiveness, these are kinks, steps, re-entrant corners and surface nucleation sites[3]. In the case depicted in Figure 10(a), there are no screw dislocations exposed on the surface neither at the twin junction nor at the crystal surface. Hence the operative growth mechanism in this case is the TPRE mechanism. In the case depicted in Figure 10(b), a screw dislocation is exposed at a twin junction; hence, preferential growth occurs at the twin junction. In this case there is growth on both sides of the crystal, i.e., the crystal grows in both forward and backward directions. In the case depicted in Figure 10(c), a screw dislocation is exposed on the surface of the crystal. As screw dislocations initiate easy surface nucleation, growth occurs on all the crystal's surfaces uniformly, and the TPRE mechanism does not contribute to growth. In the case depicted by Figure 10(d), screw dislocations are exposed at both a twin junction and the crystal surface. In this case, growth of the crystal depends on the density of screw dislocations on the surface and at the twin junction. If the density of screw dislocations at the twin junction is higher than that at the crystal surface, growth will occur preferentially along the twin junction, and the resulting crystal will resemble those that grow by the TPRE mechanism. Sunagawa et al [26] proved by means of X-ray topography that growth in quartz crystals occurs at the re-entrant corner of a

[3] Note that the effectiveness of re-entrant corners as growth sites is dependant upon the magnitude of the re-entrant angle. Small re-entrant angles are more effective than large ones. However, small re-entrant angles limit mass transfer towards the re-entrant corner. Thus a balance between these two characteristics determines the effectiveness of re-entrant corners as growth sites, and at times the effectiveness of re-entrant corners may exceed that of steps. It should also be noted that if under-cooling is excessive, surface nucleation can dominant the growth mechanism. Hence the order mentioned above is valid only for small under-cooling.

twin junction due to the concentration of screw dislocations. Extension of Sunagawa's [26] hypothesis to eutectic flake-like silicon crystals would invariably cast doubt that the TPRE is the operating mechanism in these crystals as the presence of screw dislocations at the twin junction would lead to the same kind of growth as predicted by TPRE mechanism.

Region D

At higher growth velocities and higher temperature gradients as shown in Figure 4, the silicon morphology becomes fibrous. The fibrous morphology in region D is similar to the impurity modified fibers obtained by addition of sodium or strontium. However, one important difference that distinguishes the two is the number of twins present in them. Silicon fibers in region D have very little or no twins, [23,27] while silicon fibers obtained due to additions of sodium or strontium have a large number of twins. Silicon is believed to grow isotropically at high growth rates as in region D. Isotropic growth essentially implies the effect of high interfacial energy of silicon is not active any more. Fibrous form of silicon in region D is thus a result of isotropic growth.

Primary Silicon

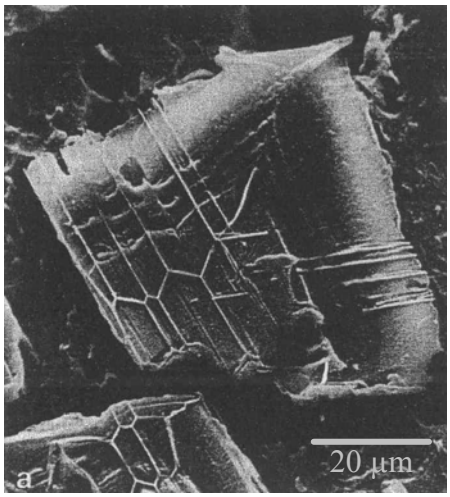

Figure 11: Primary silicon crystal with multiple twin planes [27]

Primary silicon is the pre-eutectic silicon formed in hyper eutectic aluminum-silicon alloys. Primary silicon tends to assume different morphologies like massive crystals of geometric star like or dendritic shape, complex regular silicon morphology. [27-30]

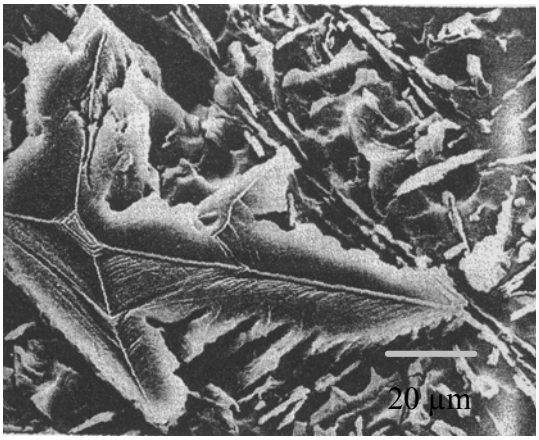

Figure 12: Dendritic primary silicon in Al-17%Si [27]

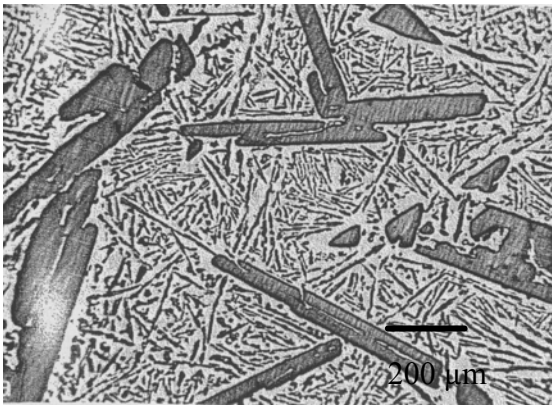

Figure 13: Primary silicon in the form of plate in Al-20%Si [27]

The predominant form in which primary silicon occurs is massive silicon. (or polygonal silicon) Massive crystals of silicon usually found in hypereutectic alloys are bounded by {111} planes. [27] Some massive crystals did not show any twinning, indicating that they were formed by layer growth mechanism on {111} planes. But most of the massive silicon crystals contain twins as shown in Figure 11. The geometry of twins in the resulting silicon does not form any specific pattern. Thus it seems that twins may not have any role to play in the growth mechanism of massive silicon. Some authors believe that the twins are formed during nucleation stage, when two embryos join together forming a twin boundary. [31-34] At higher growth velocities, the edges and corners become the preferred growth sites, leading to the formation of dendritic type silicon phase as shown in Figure 12. Higher growth velocities cause isotropic growth of silicon resulting in the formation of dendritic morphology as in metals. TPRE mechanism was found to be predominant at slow cooling rates, when primary silicon assumes plate type morphology with closely spaced twin planes parallel to the long axis, as shown in Figure 13.

2.3 Modified Alloys

Addition of some elements like sodium or strontium in trace amounts causes a change in the solidification, morphological characteristics of silicon both in eutectic and primary form. This change (specifically the morphological change) is termed as modification.

Because of its commercial importance, study of this phenomenon of modification has been the subject of intense research efforts dating back to early 1920s till today. In this section, the various changes associated with modification and different theories explaining these changes are reviewed. Sodium was used predominantly as the modifier till the late 70s, after which strontium was used. Hence the literature reviewed consists of studies on both modifiers.

2.3.1 Characteristics of Modification

In this subsection, the various changes observed by the addition of trace elements sodium or strontium is reviewed.

Effect on Microstructure

Upon addition of trace elements like sodium/strontium changes the morphology of eutectic silicon and primary silicon. Microstructural changes are discussed with respect to the different silicon morphologies observed in each region of Figure 4.

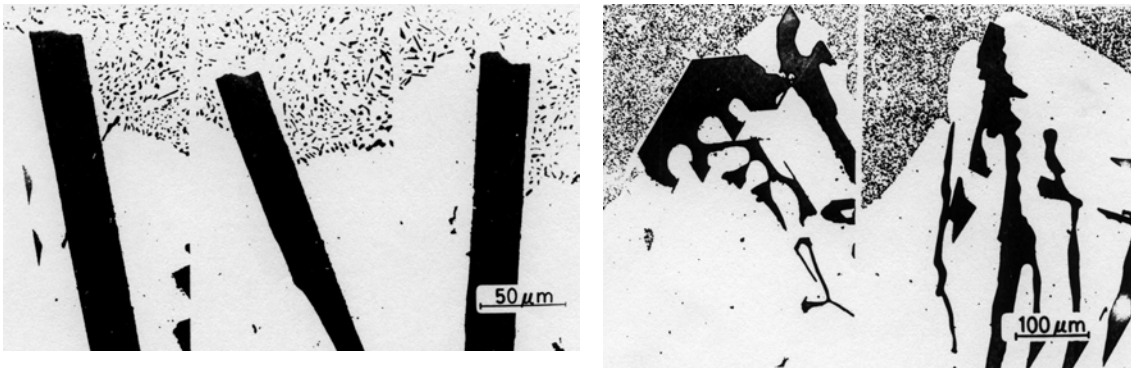

Figure 14: (a) Unmodified aluminum silicon eutectic in region A with the quench interface (b) Modified aluminum silicon eutectic (0.3%Sr) in region A with the quench interface

Platelet morphology of silicon in region A, changes into a massive irregular silicon phase. [15] Figure 14(a) shows the unmodified silicon, followed by modified silicon in Figure 14(b). Major [15] conducted directional solidification experiments with and without strontium in region A. He observed that addition of 0.03%Sr, which is usually sufficient for modification in region C did not alter the morphology of silicon. Strontium concentrations as high as 0.3%Sr was needed to obtain the morphology shown in Figure 14(b). The silicon morphology in region B, remains unaffected by the addition of sodium. [14] Flaky silicon usually observed in region C undergoes transition from flaky to fibrous morphology. At low magnifications the silicon seems spherical as shown in Figure 15(a). By deep etching and at higher magnification the fibrous morphology of silicon can be seen as shown in Figure 15b. Usually strontium quantities as little as 120 ppm would be sufficient to cause complete modification. The fibrous silicon is interconnected obviating the need to nucleate more frequently. In region D, the

regular morphology of silicon observed is itself fibrous. There is no significant morphological effect of adding strontium/sodium. Close observations with TEM, revealed that silicon in region D has a smooth surface(Refer Figure 16(a)), while in the presence of strontium the fibers are rough(Refer Figure 16(b)). An important change which takes place upon addition of strontium is with the number of twins. Fibrous silicon structure in region D has very little or no twins. But addition of strontium in region D increases the number of twins observed. [35]

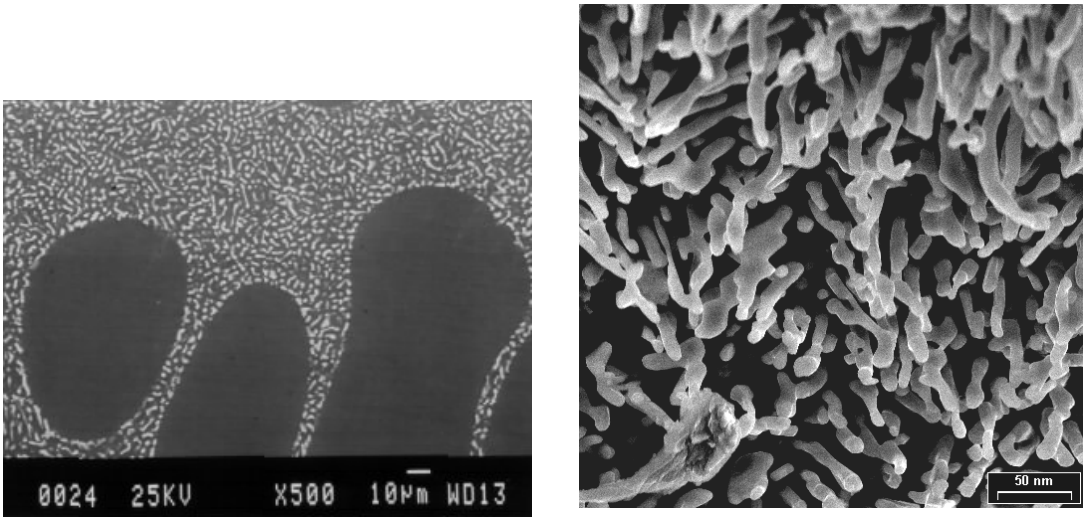

Figure 15: (a) Modified silicon at low magnifications seen as spherical particles (b) Modified silicon at higher magnification seen as fibers

Addition of modifiers to hyper-eutectic alloys changes the morphology of primary silicon from massive silicon, dendritic silicon to spherical silicon. Figure 17 shows typical spherical silicon morphology upon addition of modifiers. The spherical silicon obtained on addition of strontium/sodium is micro faceted at the external surface. The micro facets are probably the closely packed {111} planes. [29] As sodium content was increased {100} facets starts to form. [30] The re-entrant

edges observed in unmodified primary silicon are not seen in spherical silicon, indicating that sodium/strontium may be poisoning the re-entrant edges suppressing the TPRE mechanism.

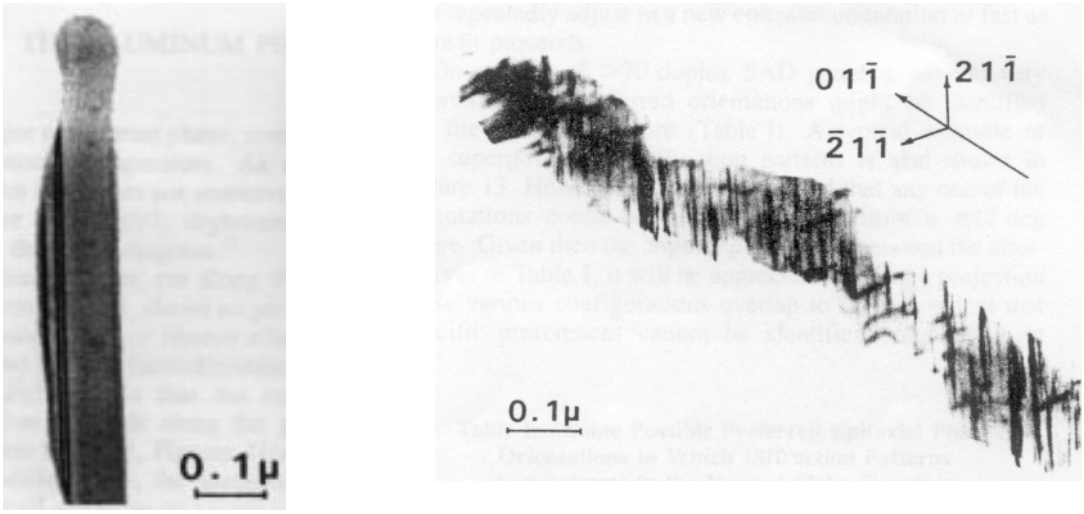

Figure 16: (a) Silicon fiber in unmodified aluminum silicon eutectic alloy obtained in region D (b) Silicon fiber in modified aluminum silicon eutectic alloy [22]

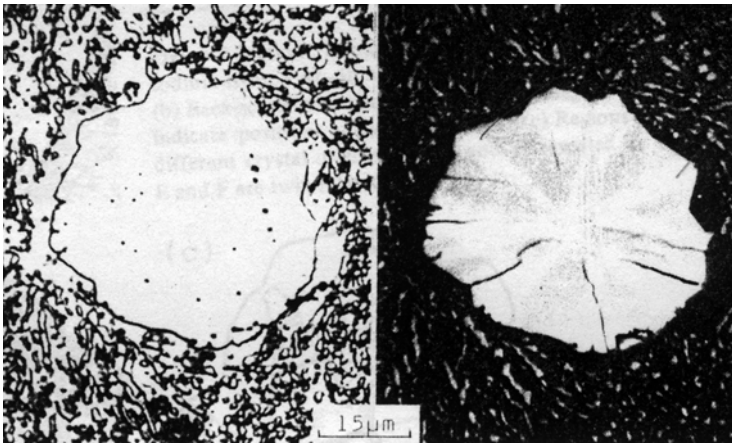

Figure 17: Spherical silicon in modified Al-16%Si alloy (a) SEM micrograph (b) Backscattered electron image Light streaks is regions of high sodium concentration [29]

Effect on Eutectic Temperature and Composition

The addition of modifiers like sodium or strontium changes the eutectic temperature and composition. The eutectic temperature is suppressed and the eutectic composition is shifted towards the higher silicon side of the phase diagram. The exact magnitude of change in eutectic temperature and composition is dependent on solidification conditions namely growth velocity (R) and temperature gradient (G). Thermal analysis of eutectic alloys [36] is shown in Figure 18(a). The eutectic temperature is clearly suppressed by as much as 6 ºK. The suppression of eutectic temperature when understood in conventional nucleation and growth theories is caused due to the suppression of nucleation. However, in this case both the nucleation temperature as well as the growth temperature of the eutectic is suppressed leading some authors to believe that change in growth is responsible for suppression of eutectic temperature. There is no consensus in the scientific community about the cause of this change in

eutectic temperature. Figure18(b) shows the change in the phase diagram upon addition of sodium, at a cooling rate of 4 ºK/min. Modifiers suppresses the nucleation of primary silicon as well, resulting in the suppression of the silicon liquidus.

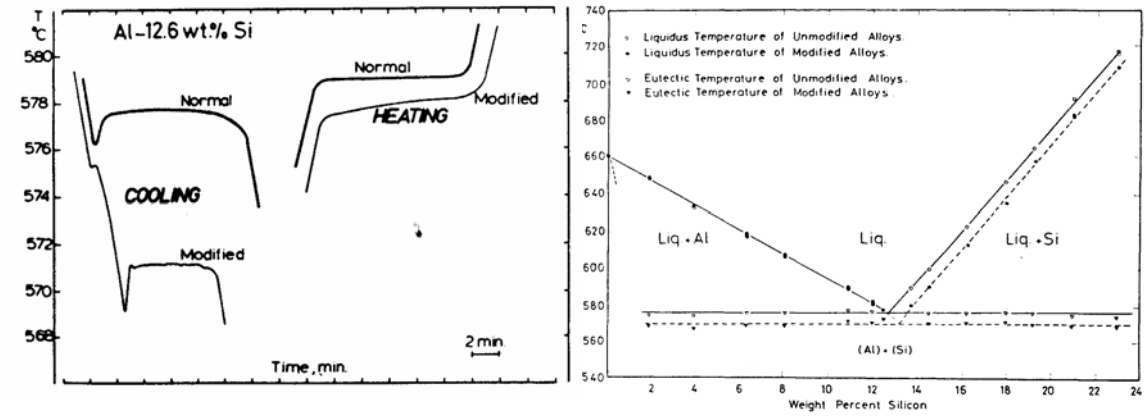

Figure 18: (a) Thermal analysis of normal and modified eutectic alloys during heating and cooling (b) Shift in the silicon liquidus and drop in eutectic temperature upon sodium addition [36]

Overmodification

Addition of large amounts of modifier (Na > 0.02% and Sr > 0.1%) causes a change in the morphology of silicon in certain regions of the microstructure. Bands of aluminum phase usually associated with coarse silicon phase are formed in the microstructure. Overmodification bands [11,37,38] were thought to be due to the formation of ternary AlSiNa phase, which nucleates coarse silicon. However, the mechanism proposed above is incorrect because overmodification

bands are not always accompanied by formation of coarse silicon particles or NaAlSi ternary compound. [38] The study of overmodification bands by the authors revealed that two kinds of bands could form, thick bands extending cross the width of the specimen and thin bands of shorter length as shown in Figure 19.

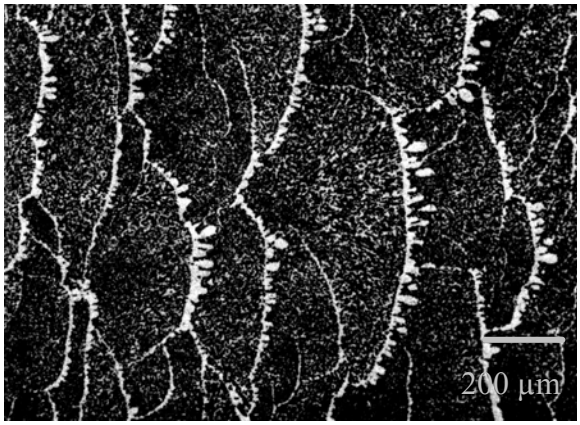

Figure 19: Overmodification bands in aluminum silicon eutectic sample. Sample obtained by directional solidification experiments at a growth rate of 120 mm/h. Thick bands with dendrites and thin bands can be observed [30]

As the rate of solidification increases the thick bands become thinner until all the thick bands completely vanish. Further increase in the solidification rates totally stops the formation of overmodification bands. The proposed mechanism [30] for this phenomenon is as follows. Growth of modified eutectic silicon stops or changes abruptly. But aluminum phase in the eutectic continues to grow resulting in a band of aluminum. The growth rate during this period becomes much less than the imposed growth rate, thus decreasing the temperature of the

solidification front. This in turn increases the driving force of formation of eutectic. Thus eutectic silicon nucleates on the overmodification band and grows rapidly into the melt. Since the temperature ahead of the overmodification band is so low, the resulting eutectic is much finer as compared to the eutectic formed prior to the band as shown in Figure 20. Various reasons have been proposed for the abrupt change in the growth of eutectic silicon before forming overmodification bands. Accumulation of very high sodium content ahead of the interface is commonly believed to be the cause. But coarse overmodification

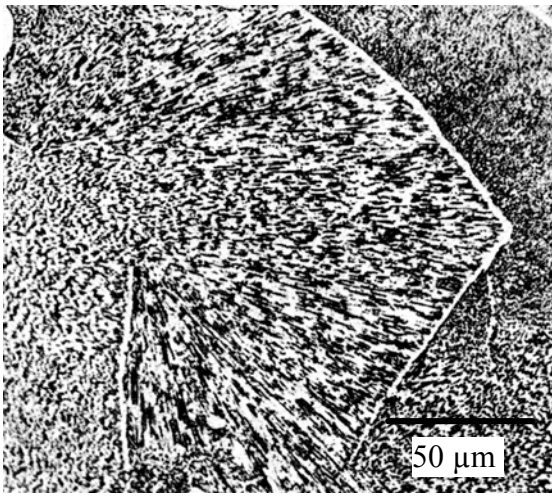

Figure 20: Overmodification band obtained in a unidirectional solidification experiment showing coarse and fine eutectic structure before and ahead of the band respectively [30]

bands (not thin overmodification bands) are always formed ahead of NaAlSi particles, where the sodium content is relatively less. The authors propose that the temperature of the interface is probably the decisive factor. As eutectic grows, sodium gets adsorbed on the surface of silicon poisoning the fast growing facets. Thus the growth rate of eutectic silicon decreases. This in turn increases

the adsorption rate of sodium. This continues till the growth is so slow that the temperature of solidification front reduces until there is a sudden nucleation of eutectic silicon. The nucleated eutectic silicon being surrounded by a melt at low temperature grows rapidly in a fine form ahead of the interface.

Effect on Porosity

Modification with trace elements is often associated with changes in porosity of the casting. [39] Unmodified castings usually have large macro pores and shrinkage. Upon modification, large macro pores are replaced with fine distributed porosity. [40] The differences in porosity distribution between a modified and an unmodified alloy have been attributed to several reasons, which are briefly discussed below.

1. The large difference in solubility of hydrogen gas in solid and liquid Al alloys (See Figure 21) causes the hydrogen gas to become entrapped in the solid, forming pores. The presence of Sr leads to increased hydrogen solubility in the melt causing more porosity. [41]

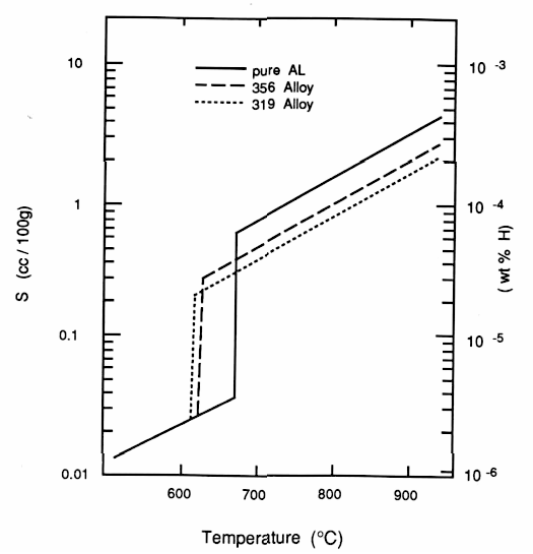

Figure 21: Solubility of hydrogen in pure aluminum and in 356,319 alloys [39]

2. Poor feedability in a casting leads to unfilled zones in the interdendritic regions causing the formation of pores. However feedability itself is affected by many parameters, such as solidification range, liquid-solid interfacial energies, feeding paths, eutectic nucleation and growth, and the volume fraction and shape of intermetallic phases. Sr is known to affect the solidification range and the liquid-solid interfacial energy of aluminum-silicon alloys, thus it can change the porosity distribution in modified Al-Si alloys. [42]

3. The presence of inclusions, such as oxides, nucleates pores and strontium based oxides act as extra nuclei for hydrogen pores. [43,44]

Studies on the change in hydrogen content upon addition of modifiers [72] using Telegas™ to measure the hydrogen content of the melt revealed no change in the hydrogen content. Hence the first possibility is ruled out. But till date complete understanding is still lacking.

Effect on Number of Twins

Modification increases the number of twins, when the flake morphology (Region C) changes into fibrous morphology. [35,45,46] The mean twin spacing in normal flake silicon is between 0.4 to 1.0 μm, while in fibers obtained by impurity addition it is as less as 5nm. [22] Thus the number of twins increase almost by a magnitude. [22,46,47] Growth direction in flake silicon is <211>, while <100> is the net growth direction in fibrous silicon. Side branching occurs only in <211> direction, which is the same as TPRE

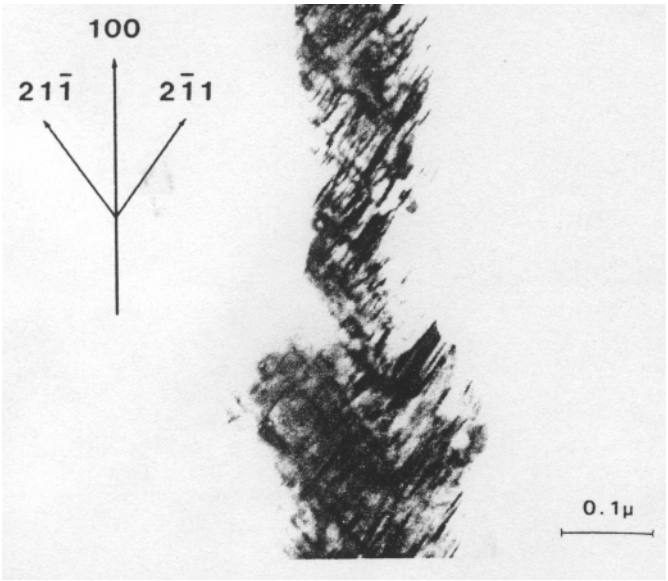

Figure 22: TEM image of modified fiber with {111} twins [22]

growth direction. [22,48] One more important difference between the two structures is the number of active twin systems. In flake silicon only two of the possible four <111> systems are active. But in fibrous silicon four <111> twin systems are observed. A typical TEM micrograph of a modified fiber is shown in Figure 22. Modification also increases the number of twins observed in the silicon in region D. Fibrous silicon obtained in region D without any modification has very little or no twins. However upon modification, the number of twins increases considerably. There has been no study on the effect of modification upon the number of twins observed silicon structures of regions A and B.

2.3.2 Theories of Modification

In this section, a review of the available theories for explaining the phenomenon of modification with respect to the characteristics is discussed. The theories are reviewed in chronological order. Along with a brief description of the theories, the experiments and the results supportive of each of the theories are discussed.

Nucleation Poisoning Theory

Nucleation poisoning theory was proposed in 1922 by Guillet [49] and also Search [50] who believed that the change in the eutectic structure with addition of sodium fluoride and potassium fluoride was due to the removal of oxides and impurities, such as alumina and silica, by the fluxing effect of these compounds. However, Curran [51] reasoned that since modification of the aluminum silicon

eutectic was also possible with metallic sodium, fluxing of impurities does not play a role in modification. However, other nuclei such as undissolved silicon, [52] aluminum phosphide [53-55] and silicon hydride [56] were thought to be potent nuclei for silicon. It was believed that sodium removes these nuclei from melt resulting in modified structure. But further experimentation of unmodified aluminum-silicon alloys with high purity metals, [57] filtration [55] and by scrubbing with an inert gas [54,58] revealed that the structure changes from granular to lamellar form and does not result in modification. In fact little additions of sodium (less than the amount required for complete modification) revealed the same change in morphology from granular to lamellar. It was believed that sodium poisons Aluminum Phosphide nuclei to result in the observed change of morphology. [37]

Ternary Eutectic Theory

In 1922, it was proposed that modification was due to the formation of an aluminum-silicon-sodium ternary alloy. [59] The modified silicon morphology was supposedly the regular morphology of this ternary eutectic. In 1924, Edwards et al [60] systematically studied cooling curves of hypoeutectic and hypereutectic aluminum-silicon alloys and found that the eutectic freezing temperature was lowered from its equilibrium value while the melting point remained at the equilibrium eutectic temperature of 577°C. This observation led them to rule out the possibility that an aluminum-silicon-sodium ternary alloy is

responsible for modification because in a ternary system the melting and freezing points coincide.

Restricted Growth Theories

Many hypotheses originating from late 1940s till today explain the process of modification as due to the restriction of growth of silicon by the impurity atoms present in the melt. However, within this genre of theories there were different thoughts as to how impurity atoms affect the growth of silicon. Change in surface energy, decrease in silicon diffusion rate, poisoning of TPRE or growth ledges were some of the possible reasons proposed. In this section, a critical review of the various hypotheses predicting restricted growth of silicon is presented.

Surface Energy Theory

In 1949, Thall and Chalmers [61] proposed a mechanism that attempted to explain chemical modification of the aluminum silicon eutectic based on the surface energy of the aluminum-silicon solid interface. They suggested that the rate of advance of the interface depends on a balance between the rate of heat flow from the liquid to the solid through the interface and the latent heat of fusion released during solidification. The thermal conductivities of aluminum and silicon in their pure form are 0.53 and 0.20 cal/cm.^{2}/$^\circ$C respectively, and their latent heats of fusion are 94.6 cal./g. and 337 cal./g. respectively. Since the difference between the magnitude of the thermal conductivity of pure aluminum and pure

silicon and the difference between the magnitude of the latent heat of fusion of pure aluminum and pure silicon are large, aluminum will solidify much faster than silicon. Thus, aluminum gains a lead during solidification of the eutectic as shown in Figure 23(a). As the cooling rate increases, the lead of aluminum over silicon increases causing

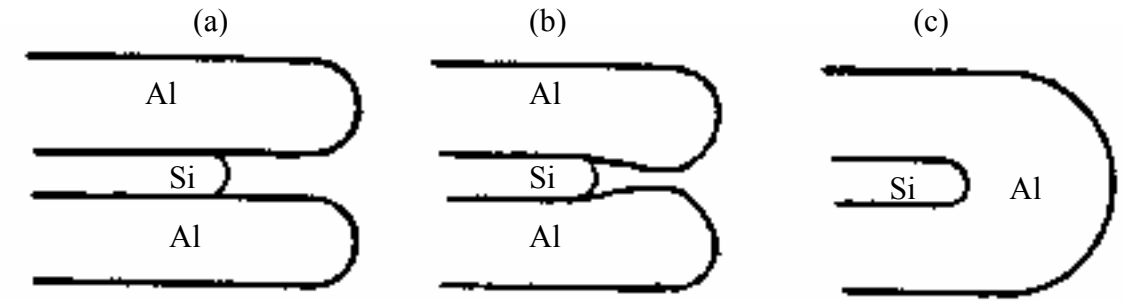

Figure 23: Eutectic solidification mechanism in unmodified chill cast alloys [61]

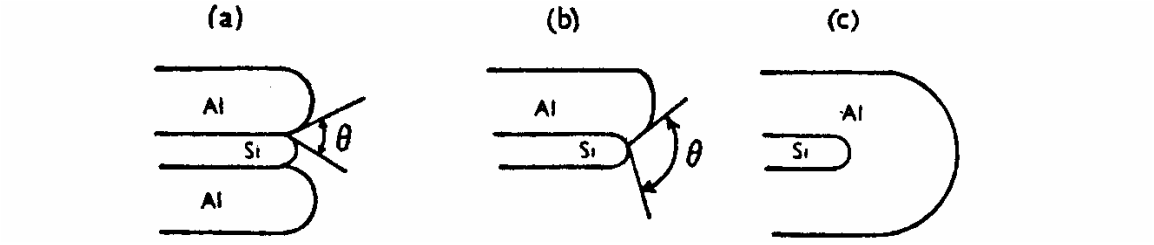

Figure 24: Eutectic solidification in sodium modified alloys [61]

complete encasement of the lagging silicon crystal by the advancing aluminum as illustrated in Figure 23(b) and 23(c). This theory accounts for the formation of

the modified eutectic structure at high cooling rates. For chemical modification, the authors suggest that a decrease in surface energy of the aluminum-silicon solid interface upon the addition of the chemical modifier increases the interface angle θ as shown in Figure 24. This in turn suppresses growth of the silicon crystal and causes modification of the eutectic structure and under-cooling. It was later proved [11,62] that addition of sodium decreases the surface tension of the eutectic liquid as shown in Figure 25. To study the effect of this change in surface tension on the interfacial angles, aluminum-silicon eutectic alloy was grown on a substrate of polycrystalline silicon with/without a atmosphere of sodium. Measurement of dihedral angles between the substrate and melt after prolonged equilibration

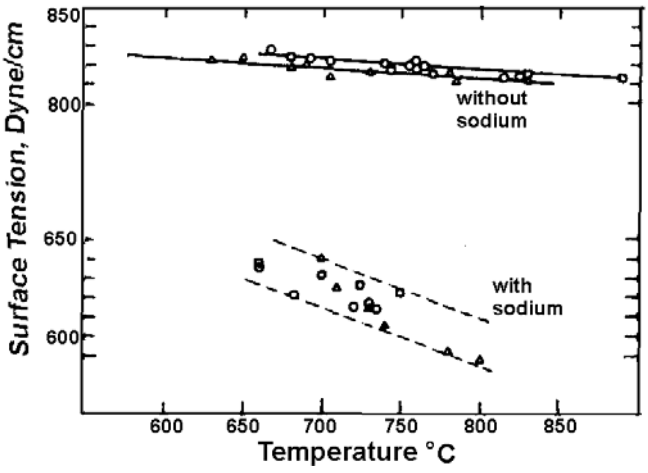

Figure 25: Surface tension of eutectic Aluminum-Silicon with and without sodium measured by maximum bubble pressure method [62]

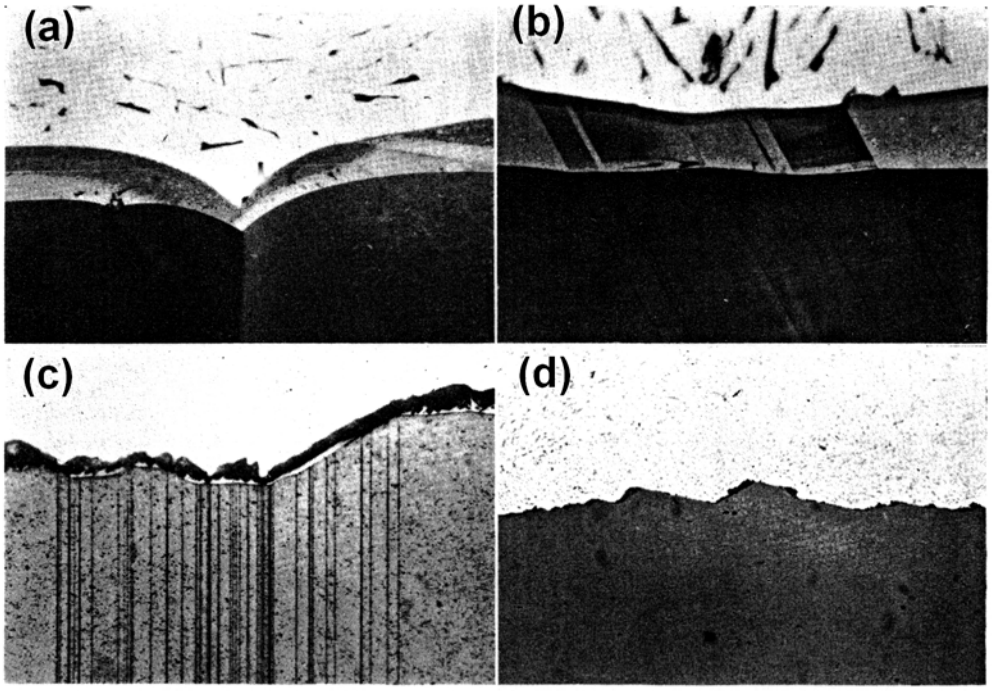

Figure 26: Growth of silicon from eutectic on a silicon substrate. (a) Grain boundary between eutectic and silicon without sodium. (b) Growth of twins from substrate into eutectic silicon in the absence of sodium (c)(d) Growth of silicon in the presence of sodium [11]

(upto 6 hours) indicated no change in the presence of sodium. Though the surface energy decreases with sodium, its inability in changing the dihedral angles, resulted in discounting the surface energy theory. However, it is unreasonable to neglect surface energy effect because of the following reasons. Surface energy plays an important role in nucleation and growth of silicon from melt, which is not exactly reproduced in the dihedral angle experiments conducted. The surface energy decreases by as much as one third of its original value upon addition of sodium (Refer Figure 25). This is a considerable decrease and neglecting the effect of surface energy cannot be justified. Moreover,

dihedral angles were measured after prolonged equilibration during which the effect of modifier on the surface energy may be lost.

Diffusion Control Theory

This theory is based on the observation that [63] solubility of sodium in solid aluminum and silicon are low. This in turn, implies that sodium would segregate ahead of the growing interface, which could restrict the diffusion of silicon in the melt. Diffusion couple experiments revealed that sodium reduces the diffusion rate of silicon. [11,63] The reduced diffusion of silicon was believed to change the growth morphology of silicon. But this mechanism was ruled out after a very careful study done by Davies and West. [11] The authors solidified an unmodified eutectic alloy in a steep temperature gradient furnace at very low cooling rates to allow enough time for silicon to diffuse. Sodium was added in the vapor form. The resulting microstructure of the sample revealed complete modification. Thus it was concluded that reduced diffusion rates of silicon has no role in modification.

Interfacial Poisoning

The idea of sodium atoms poisoning the growth sites of silicon at the interface started gaining ground. One of the first experiments to prove this idea was performed by Davies and West [11]. Unmodified aluminum silicon eutectic alloy was vacuum cast upon a pure polycrystalline silicon substrate by a bottom pour technique with/without an atmosphere of sodium. They observed that growth of

silicon in the presence of sodium was negligible as compared to silicon growth in its absence (Refer Figure 26). Moreover, silicon tends to be faceted in the presence of sodium. Thus sodium not only seems to reduce the growth rate of silicon but also makes silicon more faceted.

Among the theories, which believe interfacial poisoning of silicon at the interface causes the decrease in growth rate of silicon, there were two different trains of thought. One group of researchers believed that interfacial poisoning of re-entrant edges of TPRE mechanism by modifier atoms is responsible for modification. While another group believed that interfacial poisoning takes place by poisoning of growing ledges of silicon. Both of these hypotheses are reviewed further and their pros and cons discussed.

TPRE Poisoning

Detailed TEM studies [23,46] of the impurity modified silicon morphology revealed the growth mechanism of fibers. Figure 27 shows the twin traces of a modified fiber. Figures 27a and 27b show the bright field images, while Figures 27c and 27d show the dark field images of the same fiber. The growth of silicon is in a zig-zig fashion. Study of electron diffraction patterns of the fibers revealed the growth mechanism, which is shown schematically in Figure 27(e). The AB twins in the left bottom of Figure 27(e) gives rise to branching in the form of BC twins through multiple twinning. Further AB twins are in $[11\bar{2}]$ direction, while the BC twins are in $[\overline{112}]$ directions. From the observation that each fiber in the

impurity modified silicon fiber grows in the [112] direction, it was believed that growth in impurity modified fiber is also by TPRE mechanism.

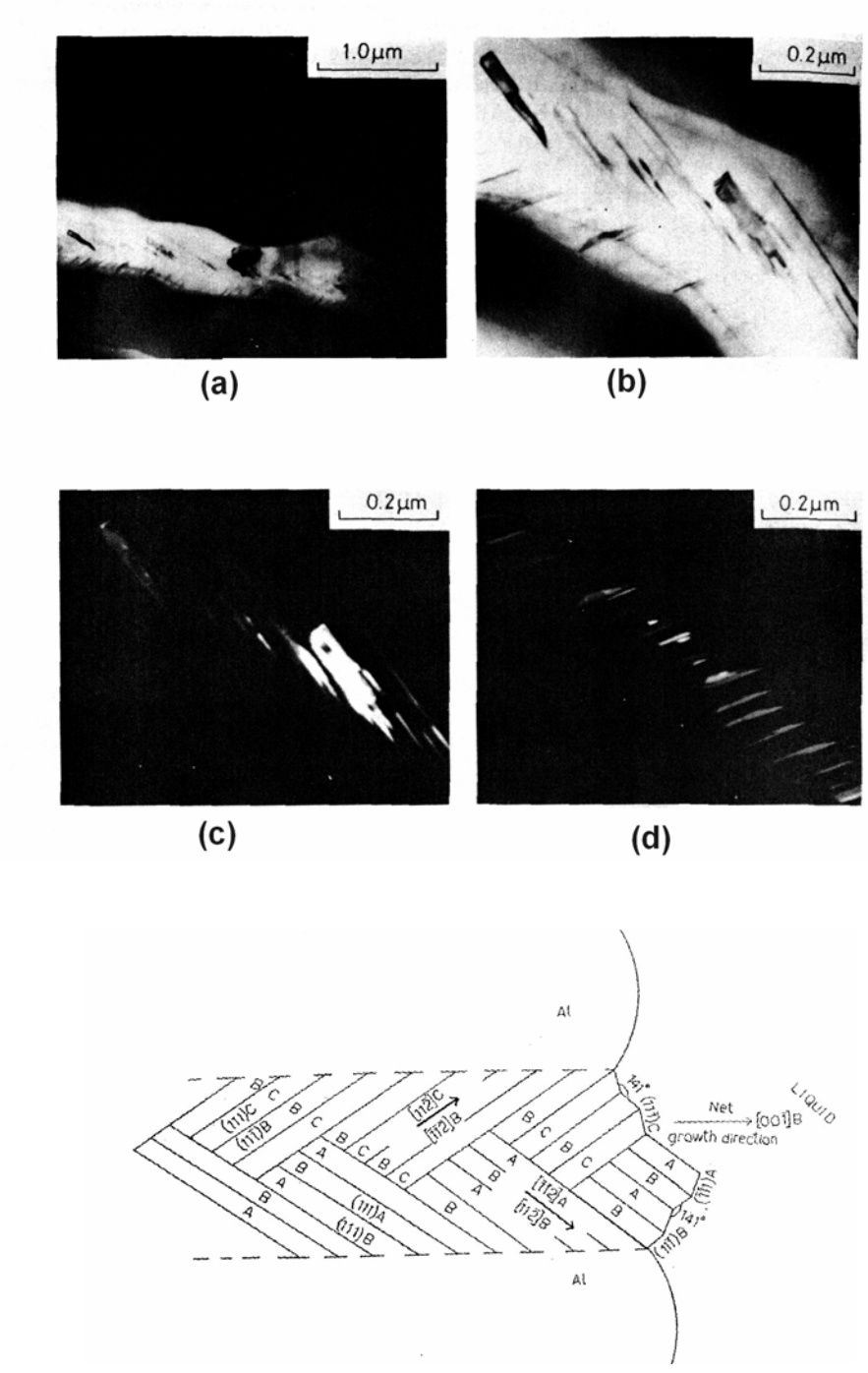

Figure 27: Growth of modified silicon fiber in Al-14%Si-0.18%Sr alloy (v=330 μm/s and G = 50□C/cm) (a) (b) Bright field images (c) (d) Dark field

images (e) Schematic of twins and their growth directions in a modified silicon fiber [46]

But modifier atoms poisoning its re-entrant edges supposedly stop the growth by TPRE mechanism. Because of the impurity atom poisoning, the fiber changes its direction by multiple twinning often resulting in coral type morphology. This hypothesis of TPRE poisoning mechanism does not exactly predict how exactly the poisoning of re-entrant edges takes place and what characteristics determine whether an element can act as a modifier. However, the most important question that TPRE poisoning hypothesis fails to answer is the reason why modifiers fail to change the silicon morphology in region B as it is known to contain {210} twins. [64,65]

Impurity Induced Twinning

To explain the modification due to impurity elements, Shu-zu-lu and Hellawell proposed [22] a theory (Impurity Induced Twinning theory) that the modifiers like sodium or strontium could act as a poison to already growing atomic layers. Here the impurities are assumed to adsorb to the step or kink sites, thus preventing attachment of atoms or molecules to the crystal as shown in Figure. 28.

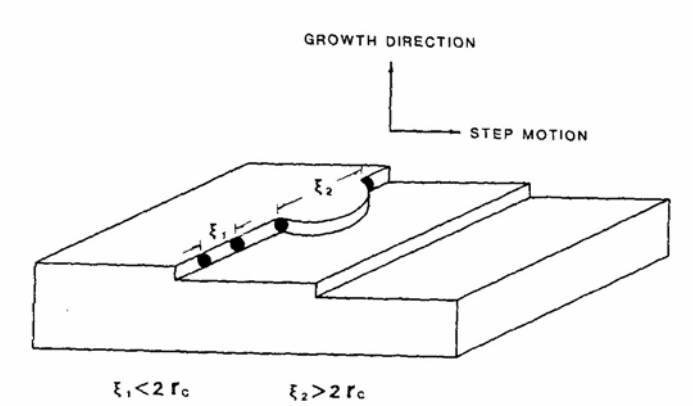

Figure 28: Schematic of impurity atoms pinning the steps of silicon crystal growing by layer growth at the interface [22]

Further these poisoning atoms could induce twinning by altering the stacking sequence of atomic layers in order to grow around the impurity. Based upon this premise, the authors calculated the ratio of impurity to matrix atom radii required for impurity induced twinning to be r_i/r_{Si} = 1.6457 assuming an FCC lattice. The plot of atomic radius versus atomic number of various elements with the shaded region that within which an element should be capable of inducing twinning in silicon is shown in Figure 29. Qualitative analysis for sodium in the modified alloys using auger electron spectroscopy [22] and electron micro probe analysis [47] indicated segregation of sodium in the silicon fibers and in aluminum. The authors consider this to be a validation of the Impurity Induced theory. Directional solidification experiments with aluminum silicon alloys in the presence of sodium at high growth rates (in region D) were conducted. The 'doubly' modified fibers showed a high multiple twin density similar to sodium modification at lower growth rates. Thus, increase in twinning due to impurity modification is independent of the growth rate. In the following section the

various aspects of Impurity Induced Twinning model is discussed with respect to the available evidence in the literature.

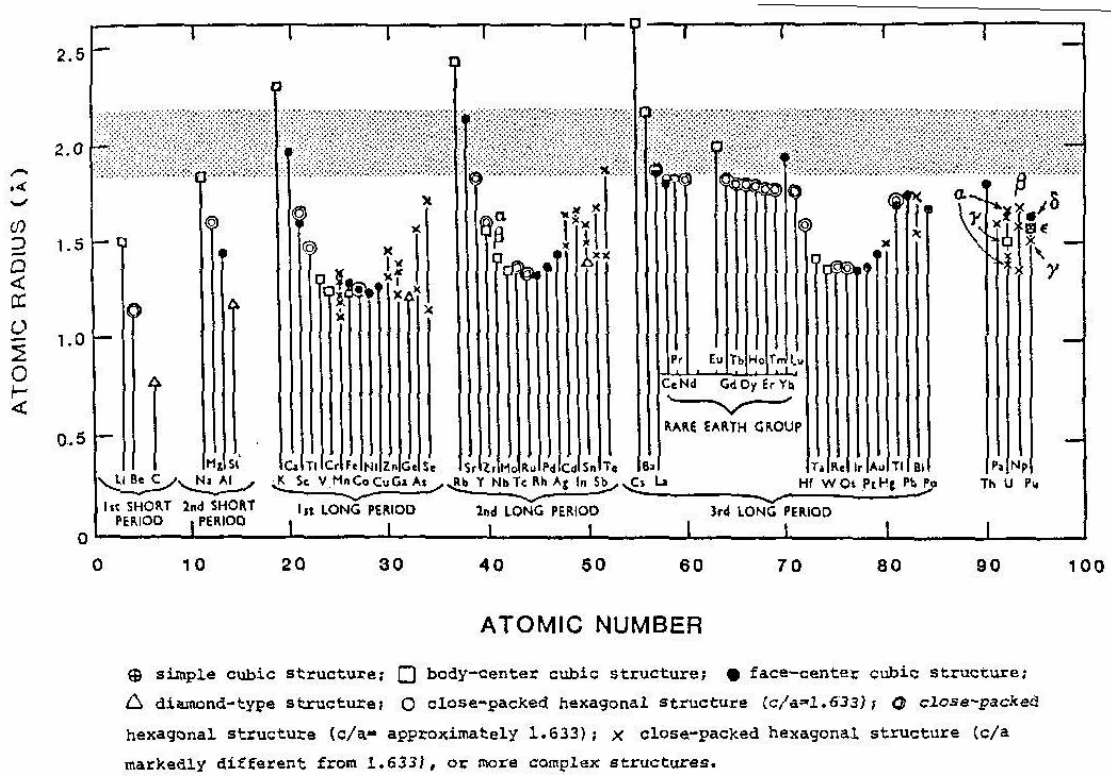

Figure 29: Plot of atomic radii versus atomic number. The range of atomic radii (as predicted from hard sphere model) capable of modifying the silicon structure is indicated as a band [22]

One of the basic premises underlying Impurity Induced Twinning theory is that flake silicon grows predominantly by layer growth and not by TPRE mechanism. Layer growth of silicon flakes does not explain the plate shape morphology formed in unmodified alloys. If layer growth on {111} planes of silicon were to be predominant, there should be lateral growth on the flakes of silicon, which certainly is not observed. Moreover, TPRE mechanism in silicon growth has

been shown to be predominant in several of the previous studies. Fred Major [15] conducted directional solidification experiments of aluminum-silicon eutectic at ultra low growth rates, which clearly showed the operation of TPRE mechanism in region A of unmodified alloys and the absence of it in Sr modified alloys. Flakes of silicon were mostly observed to contain a minimum of two twins and singly twinned plates were very rarely observed. The authors who believe that layer growth is dominant in growth of unmodified silicon explain the presence of twins as due to thermal stresses. If twinning in silicon were due to stresses between aluminum and silicon, the probability of finding a singly twinned silicon flake should be the same as doubly or triply twinned silicon flake. These observations cast a serious doubt that flake silicon grows by layer mechanism and not TPRE.

Sodium, which is less than the ideal radius ratio as predicted by Impurity Induced Twinning, is a better modifier than ytterbium or calcium, which are close to the ideal ratio. Moreover, lithium which is no where close to the ideal ratio has been shown to modify when added in large concentrations. [66] However, if the impurity element affects only layer growth mechanism as supposed in Impurity Induced Twinning model, it explains why strontium does not affect the silicon morphology of region B, inspite of containing {210} twins.

3. DESIGN OF EXPERIMENTS AND PROCEDURES

In this section, the design of various experiments, conducted to further our understanding of the evolution of aluminum silicon eutectic will be discussed. Various parameters used in the experiments along with the materials used to conduct the experiments are also discussed. It is followed with a step by step description of the procedures used in the experimentation.

Several experimental approaches were simultaneously undertaken to study the evolution of the eutectic microstructure. A multi-pronged approach was necessary because of the number of issues that needs to be resolved in order to arrive at a comprehensive understanding of this complex phenomenon. The following is the list of the experiments conducted in this study.

- Nucleation and growth of the eutectic and the influence of phosphorous were addressed using quench experiments for both commercial purity alloys and high purity alloys.

- The role of interfacial energy in dictating the morphology of the eutectic and determining the porosity was studied by performing sessile drop experiments.

- Thermal analysis and microscopy of unmodified and Sr modified Al-Ge system was investigated, as it is analogous to the Al-Si system.

- The effect of modifier (Sr and Na) additions on the hydrogen content of commercial alloys was performed in order to address the issue of increased porosity levels in modified castings.

The design and the procedures of each of the above mentioned experiments are discussed in detailed in the following sections.

3.1 Quench Experiments

3.1.1 Design of Experiments

High purity hypoeutectic alloys of the required compositions were prepared. Thermal analysis of the alloys was performed and the cooling curves were used to determine the temperature at which the eutectic nucleates and the time over which the eutectic plateau extends. The quench experiments involve cooling the alloy from 750°C slowly to the eutectic nucleation temperature (as determined from thermal analysis) and quenching in a quench solution, after various times in the eutectic plateau. The quench liquid has a very fine microstructure and hence can be distinguished from the quasi-equilibrium eutectic. Analyzing the quenched samples using optical microscopy and SEM allows locating where the eutectic nucleates.

The various alloys that will be tested include high purity Al-Si alloys with and without Sr and/or P. In order to study the effect of varying volume fraction of

primary aluminum on the nucleation of eutectic, two alloys, one having very high volume fraction of primary aluminum Al-(5-6%) Si and the other having a higher volume fraction of eutectic Al-(10-11%) Si are chosen. The amount of strontium used for modification is 0.02wt% for the Al-(5-6%) Si alloy and 0.03% for Al-(10-11%)Si alloy. The various parameters used in the experiment are listed in Tables I and II. For the sake of comparison two commercial purity alloys were also studied.

Table I: Constants

Parameter	Magnitude or Type
Cooling Rate (thermal analysis)	1°C/min
Cooling Rate (before quenching)	1°C/min
Quench Media	Ethylene glycol and water (1:1) cooled to -40°C by dry ice
Holding temperature	750°C

Table II: Variables

Variables	Magnitude	
Silicon	5-6wt%	10-11wt%
Phosphorous	0.0	0.0003
Strontium	0.0	0.02
Quench Time	10,40% of eutectic plateau	

Materials

High purity aluminum (99.999% purity) in the form of ingot and 99.9999% purity silicon in the form of small particles were used. Strontium was added in the form of Al-9.99%Sr master alloy. Phosphorous was added in the form of Al-19Cu-1.5%P master alloy. Alumina crucibles were used for thermal analysis, quench experiments and alloy preparation.

3.1.2 Procedure

Alloy Preparation

Alloys were prepared in a Thermolyne box furnace. The high purity aluminum of required amount was cut into small blocks. Aluminum blocks were then ground on 60 grit silicon carbide paper and cleaned in ethanol in an ultrasonic vibrator to remove any surface impurities. The silicon particles were also ultrasonically cleaned in ethanol to remove impurities. The aluminum was first melted and maintained at 800°C. The silicon was then added into the melt and stirred using a graphite rod. The alloy was allowed to solidify as soon as the silicon diffused into the melt. Strontium additions and phosphorous additions were made at the end. The alloy was allowed to solidify in the furnace to minimize oxidation. The resultant alloy was analyzed by wet analysis at Henry Yeager laboratories, PA to determine the composition including the phosphorous content.

Thermal Analysis

Approximately 40 grams of the alloy was taken in a alumina crucible and heated to 750°C. The sample was held at 750°C until the furnace and the melt were in equilibrium. The sample was cooled at a rate of 1°C /min. The temperature was measured by a K-type thermocouple of 0.4mm thickness placed at the center of the crucible. The thermocouple was connected to a data acquisition system, which was connected to a computer running Labview software. Data was collected every tenth of a second until the alloy completely solidified.

Quench Experiments

The alloy was melted in the same furnace and in the same size crucible as in the thermal analysis experiments to simulate the same cooling curve as generated during thermal analysis. The alloy was allowed to cool down at 1°C/min until it reached the eutectic temperature. At the appropriate time in the eutectic plateau, the crucible was dropped into the quench solution that was maintained at -40°C. Samples from the quenched ingot were taken close to the thermocouple location. These samples were prepared for microstructural analysis using standard metallographic techniques. The samples were viewed un-etched and etched. Electropolishing was used for deep etching to observe silicon morphology.

Table III: Chemical analysis of high purity alloys

Alloy		Si (wt%)	P (wt%)	Sr (wt%)
1	Target	6 - 7	0	0
	Achieved	10 - 11	0.0007	<0.0001
2	Target	10 - 11	0	0
	Achieved	11.18	0.0003	<0.0001
3	Target	6 - 7	0	0.03
	Achieved	6.66	0.0007	0.029
4	Target	10 - 11	0	0.03
	Achieved	10.4	0.0004	0.031
5	Target	6 - 7	0.003	0
	Achieved	6.52	0.0019	<0.0001
6	Target	10 - 11	0.003	0
	Achieved	10.72	0.0023	<0.0001
7	Target	6 - 7	0.003	0.03
	Achieved	6.52	0.0019	0.028
8	Target	10 - 11	0.003	0.03
	Achieved	10.72	0.0023	0.029

Microstructure Analysis

Deep etching was performed in a Buehler electromet III electro polisher. The electrolyte used was ethanol (95 percent) 700ml, 2-butoxy ethanol 100ml and perchloric acid (30 percent) 200ml. Electro polishing was performed at 15V for 5 seconds. During electro polishing, the reagent reacts preferentially with aluminum dissolving it and leaving silicon behind in the eutectic.

The Microstructures were examined using a variety of techniques including optical microscopy, image analysis, scanning electron microscopy (SEM) and Energy Dispersive X-ray (EDX) analysis. Numerous aspects of the microstructure were examined, including the origin of the eutectic phase, the eutectic grain morphology.

3.2 Sessile Drop Experiments

Commercial hypoeutectic Al-Si alloys consist of essentially two phases: primary aluminum and the eutectic. During the solidification of hypoeutectic alloys, primary aluminum forms first in the form of dendrites, followed by the eutectic. During the formation of the eutectic, primary aluminum is readily available as heterogeneous nucleation sites. The capacity of primary aluminum to act as a heterogeneous nucleation site for the eutectic depends on the interfacial energy between primary aluminum and the eutectic liquid. The interfacial energy also determines the faceting tendency of silicon and the effect of sodium and strontium on the faceting tendency of silicon. Thus, studying the interfacial energies of unmodified/ modified eutectic and primary aluminum also helps in understanding the growth of silicon and thus mechanism of modification. [61,67,68]

Another important parameter during casting of Al-Si alloys is feedability. Feedability becomes important in Al-Si alloys once the dendrites impinge on each other and form an interconnected solid network. [69,70] The last liquid fraction to solidify is of eutectic composition. The eutectic liquid now has to flow

through channels between the dendrites and grains. The ability of the eutectic to flow over the network of dendrites depends on the wetting behavior between the eutectic and the primary aluminum. When the driving force of a eutectic alloy to wet the primary aluminum is high, it is easier for the liquid to flow over the dendrites and better feeding is attained causing a measurable reduction in porosity. Thus, the determination of driving force of the eutectic (unmodified/modified) to wet the primary aluminum, would lead to the understanding of wetting characteristics of modified and unmodified melts. Determination of interfacial energy between eutectic (modified/unmodified) and primary aluminum is essential in estimating the driving force to wet of a modified and unmodified eutectic on the primary aluminum.

3.2.1 Design of Experiments

Experiments conducted in this study used a substrate of Al-1%Si. Reasoning behind using Al-1%Si is that it represents the typical composition of a primary aluminum dendrite in contact with eutectic liquid in hypoeutectic alloys. The experiments were conducted at eutectic temperature to simulate the exact condition in a casting, where the eutectic has to flow over the dendrites to feed. Thus, the results from such experiments would guide us to understand the wettability of dendrites by modified vs. unmodified eutectic melt and thus feedability and porosity formation in these alloys.

3.2.2 Materials

Three different alloys of eutectic composition, unmodified, modified with sodium and modified with strontium were prepared in an induction furnace, using 99.8% purity aluminum and Al-50%Si master alloy. The amount of silicon in the alloy was adjusted until the exact eutectic composition was obtained. The modified eutectic was adjusted to 13.1% silicon because of the shift in eutectic on addition of modifiers. Strontium was added in the form of Al-10%Sr master alloy and sodium was added as metallic sodium. Apart from the eutectic alloys, an alloy of Al-1%Si composition was also prepared. Composition of the alloys is listed in Table IV.

Table IV: Chemical analysis of substrates and sessile drops

Substrate	Al-1%Si Machined Alumina plate
Sessile drops	Al 12.6% Si Al –13.1%Si – 0.04%Sr Al – 13.1%Si – 0.02%Na

3.2.3 Experimental Apparatus

A schematic of the apparatus is shown in Figure 30. A high temperature horizontal tube furnace with a 6.5 cm diameter alumina tube was used for the experiments. The alumina tube was closed at both ends with end-cap fittings. Both end-cap fittings were sealed with O-rings and are capable of maintaining a vacuum of atleast 3.5×10^{-2} atm. A K-type thermocouple was inserted in one end of the tube, while at the other end an optical window was used to allow video recording. An atmosphere of ultra high purity argon gas was used to avoid

oxidation of the alloy. The entire experiment was video recorded using an S-VHS camera for better resolution. The analog tapes were converted to digital files using Dazzle videocreator™ software. Snapshots of the digital video files at the requisite instants were used to get the profiles of the sessile drops. The interfacial energy and driving force to wet were calculated using empirical equations available in the literature. Appendix 1 details the science behind interfacial energy (or surface tension) and empirical equations for calculations using sessile drop experiments. The time taken for complete wetting of the droplets on Al-1%Si was also recorded.

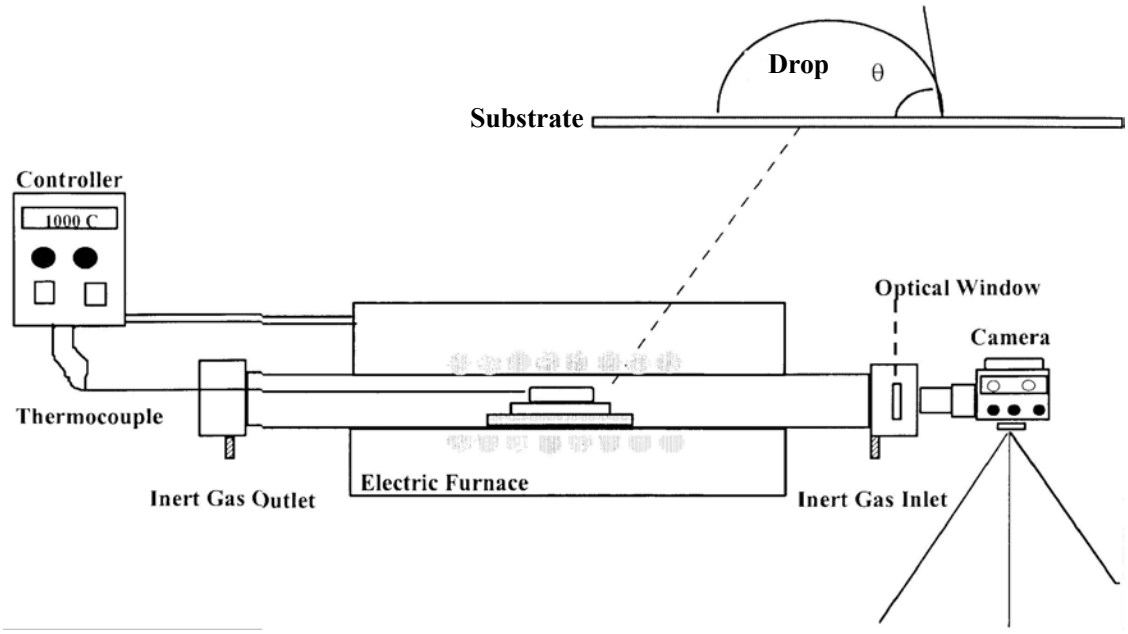

Figure 30: Experimental Setup for Sessile drop experiments

3.2.4 Experimental Procedure

Prior to the experiments, cubic pellets weighing 6 ± 0.1gms were cut from the ingot. To prevent oxidation the cubic pellets and Al-1%Si substrate used in the

experiments were freshly ground on 240 and 400 grit silicon carbide papers. The specimens were ultrasonically vibrated in a solution of ethyl alcohol for five minutes and were removed out of alcohol only before the experiment. The cubic pellets were placed on the substrate and were carefully inserted into the tube furnace. The flow of argon gas was started 10 minutes before the start of experiments to flush out the air. The specimens were heated at the rate of 15^{o}C/min till the eutectic temperature was reached. Temperature was monitored with an external thermocouple inserted into the tube furnace and placed close to the substrate. When Al-1%Si was used as the substrate, experiments were continued till the eutectic droplets completely wetted the surface. But in the case of alumina substrate, the temperature was raised till 800^{o}C after the formation the droplets to observe the occurrence of wetting if any.

All the experiments were performed with two alloy pellets, one modified and one unmodified, placed together on a substrate. For sodium and for strontium-modified alloys, three such runs were performed. Two runs were performed using an Al-1%Si substrate, and one using an alumina plate.

3.3 Study of Analogous System: Al-Ge System

The Al-Ge system was investigated because of its similarity to the Al-Si system. If the results of this study were different from what we expect from our understanding of the Al-Si system, it would help us revisit our understanding and improve our knowledge of microstructural evolution in Al-Si system.

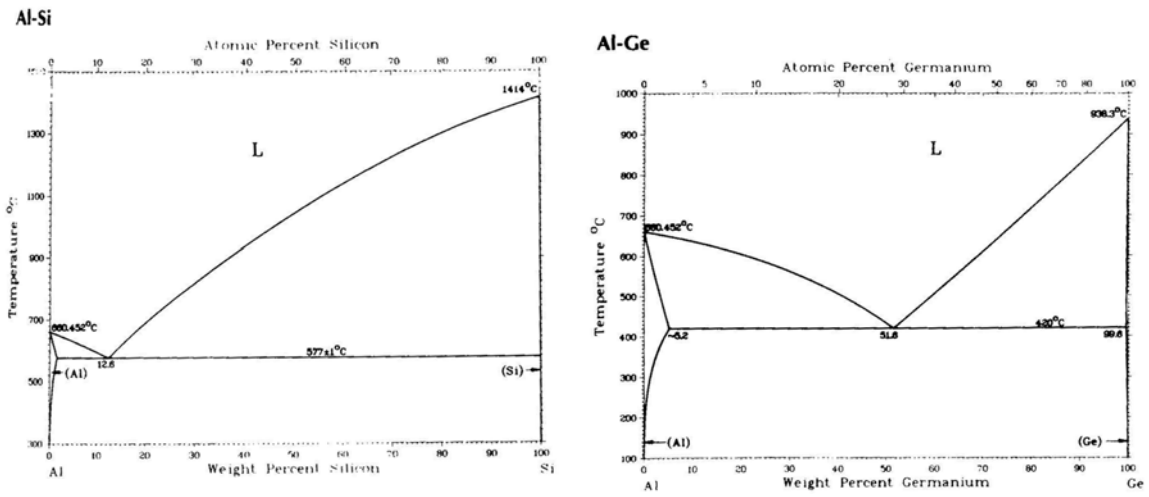

Figure 31: Binary phase diagrams of Al-Si and Al-Ge

Figure 31 shows phase diagrams of the aluminum-silicon and the aluminum-germanium systems. Both systems are simple eutectic. Both germanium and silicon have the same crystal structure, namely diamond cubic, and the same space group, namely Fm3m. The atomic radii of the germanium and silicon atoms are 1.37 A and 1.32 A respectively. Like silicon, germanium grows by the TPRE mechanism.[3] However, it should be pointed out that the eutectic composition in the Aluminum germanium system is 51.6% germanium, much higher than the aluminum-silicon eutectic.

3.3.1 Experimental Procedure

Two hypoeutectic alloys of Al-Ge were prepared with high purity aluminum and germanium (99.999%). The composition of the alloys was Al-20Ge and Al-20Ge-0.04%Sr. Experiments were carried outperformed in a box furnace. The aluminum was melted in an alumina crucible at 700°C. Germanium was added to the melt and was held for 30 minutes to completely diffuse and the alloys were

solidified. Thermal analysis was performed using Labview data acquisition system. Microscopy was performed using optical and scanning electron microscopy.

3.4 Effect of Strontium Addition on Hydrogen Content

The aim of this set of experiments was to understand the change in porosity upon addition of modifiers. Though sessile drop experiments helped in evaluating the wettability of eutectic melt over the surface of primary aluminum, many investigators [41,42,71,72]believe that strontium affects the hydrogen content in the melt. Moreover, the results of sessile drop experiments indicated the change in interfacial energy upon addition of strontium. Interfacial energy of the melt has an important role in the nucleation of hydrogen gas melts as can be seen from equation (1), which is the pressure balance equation for a stable bubble. [73]

$$P_g = P_o + \rho_L g_r h + \frac{2\sigma_{gL}}{r} \qquad (1)$$

where P_g is the total gas pressure in the bubble, P_o is the ambient pressure, $\rho_L g_r h$ constitutes the metallostatic pressure head and the final term is the pressure in the bubble resulting from the bubble-melt interfacial energy σ_{gL}. For a constant total gas pressure P_g, if the interfacial energy σ_{gL} decreases the radius of the bubble required to form a stable bubble also decreases. Thus, a decrease in interfacial energy would mean easier bubble nucleation. Thus it was felt that in-situ measurement of hydrogen gas upon addition of modifiers to the

melt was performed. Lack of relevant data in the literature using the latest in-situ hydrogen measurement device Alscan™ (Refer Appendix II) also provided the motivation to perform the following experiments.

3.4.1 Experimental Procedure

Experiments were performed on two different commercial aluminum silicon alloys, namely 319 and 380. Typical composition of alloys used in the experiments is listed in Table V.

Table V: Typical composition of 319 and 380 alloys used in Hydrogen measurements

Alloy	Si	Fe	Cu	Mn	Mg	Zn	Ti
319	5.9	0.8	3.4	0.31	0.12	1.1	0.13
380.1	9.0	1.1	3.6	0.24	0.057	2.52	0.053

About 35 lbs of melt were prepared for each run. Melting was performed in silicon carbide crucibles in an induction furnace at 750°C. The melt was then transferred to an electric holding furnace set at 700°C and allowed to equilibrate with the furnace temperature.

About 3 hydrogen measurements were taken over a period of 30 minutes using Alscan™ in the unmodified melt. Details of the working principle of Alscan™ device are elaborated in Appendix II. Strontium was then added in the form of Al-10%Sr master alloy rods. The master alloy was dropped into the melt without

any stirring in order to avoid hydrogen intake from the atmosphere. The probe stirring in the Alscan™ was sufficient for homogenous mixing of Sr in the melt. A spectroscopy sample was collected and Alscan™ reading were started. Hydrogen measurements were made until there was no appreciable change in hydrogen in the melt with further time. At the end of the experiments another spectroscopy sample was collected.

In order to examine the correlation between modification and hydrogen content, 3 levels of strontium were used for each alloy: 0.002% for partial modification, 0.04% for complete modification and 0.1% for over modification.

3.4.2 Metallography

Samples for metallography were collected after the addition of strontium. The samples were prepared using standard microstructural procedures as described earlier. Microstrutural analysis was done by using optical microscope and a JEOL 840 scanning electron microscope.

4. RESULTS AND DISCUSSION

In this section, the results obtained in each of the four different sets of experiments will be presented, followed by the discussion of the results. Since the results of each of the experiments are inter-related with other experiments, apart from the discussion for individual experiments a final discussion combining the results of all experiments is presented at the end of this section.

4.1 Quench Experiments

The results of quench experiments with various high purity alloys are discussed in this section. The results are presented and discussed under various aspects such as Thermal analysis, Nucleation of eutectic, Growth of eutectic especially silicon, leading phase at the interface, Macro structural growth mode and effect of phosphorous on the microstructure. The effect of modifier (strontium) is discussed within each of these topics to directly study the changes brought upon by addition of modifiers.

4.1.1 Thermal Analysis

The thermal analysis of all the eight alloys was performed at the rate of 1 ºC/min**.** The cooling curves were analyzed and important parameters such as liquidus temperature, eutectic temperature and width of eutectic plateau have been measured. The results are shown in Table VI.

Table VI: Thermal analysis of high purity alloys

Alloy	Liquidus Temperature (°C)	Eutectic Temperature (°C)	Time in Eutectic Plateau (Sec)
Al - 6.74 %Si	612.4	577.5	1275
Al – 11.1%Si	585.2	576.6	3343
Al – 6.6 %Si – 0.029%Sr	608.3	572.8	1418
Al –10.4%Si – 0.03%Sr	583.5	573.1	3520
Al – 6.52%Si – 0.019%P	612.3	574.1	1390
Al – 1072%Si – 0.023%P	586.6	573.7	4408
Al – 6.52 %Si – 0.0019 %P – 0.028% Sr	615.0	573.7	1420
Al – 10.72 %Si – 0.029%Sr	591	575.2	4300

The eutectic plateau temperature of high purity alloy Al-6.74%Si is close to the theoretical eutectic temperature namely 577 ºC. But upon addition of 0.03%Sr the eutectic temperature decreases to 572.8 ºC. The decrease in the eutectic temperature upon addition of strontium is well known. There is no unanimously accepted explanation for this phenomenon in the literature. Among the various explanations explaining this phenomenon, suppression of eutectic growth and suppression of eutectic nucleation are the important ones. However, it is believed that suppression of eutectic nucleation is the reason for decrease in eutectic nucleation. Further evidence for suppression of eutectic nucleation is presented in the next few sections.

The effect of phosphorous on the eutectic temperature cannot be ascertained from the data obtained here, because phosphorous was added in the form Al-19Cu-1.5%P master alloy containing copper. Thus copper was added as an unwanted impurity in the alloy. The eutectic temperature of phosphorous containing alloys show a decrease in the eutectic temperature. This decrease in eutectic temperature is probably because of the presence of copper in the alloy. The eutectic temperatures in modified alloys containing phosphorous have a typically higher eutectic temperature than modified alloys without phosphorous. This can be explained on the basis of phosphorous poisoning the modifying effect of strontium. [68,74] The time in eutectic plateau gives an indication of the volume fraction of eutectic present in the alloy. In this experiment hypoeutectic alloys of two different volume fractions were chosen. Alloys with 6-7%Si contain about 30% volume fraction of eutectic, while alloys with 10-11%Si contain 70% volume fraction. The length of eutectic plateau (indicated as time of eutectic plateau) is thus more for a 10-11%Si alloy than a 6-7%Si alloy.

4.1.2 Nucleation of Eutectic

In this section, the results pertinent to the nucleation of eutectic at microstructural scale and macrostructural scale are presented. First the results of unmodified alloys followed by modified alloys are presented. Figure 31 shows the microstructure of Al-6.74%Si alloy quenched at 10% of the eutectic plateau. The coarse silicon is formed at slow cooling at the eutectic temperature. The

fine eutectic is the eutectic formed during quenching. Close observation of the coarse silicon indicates where the eutectic has nucleated.

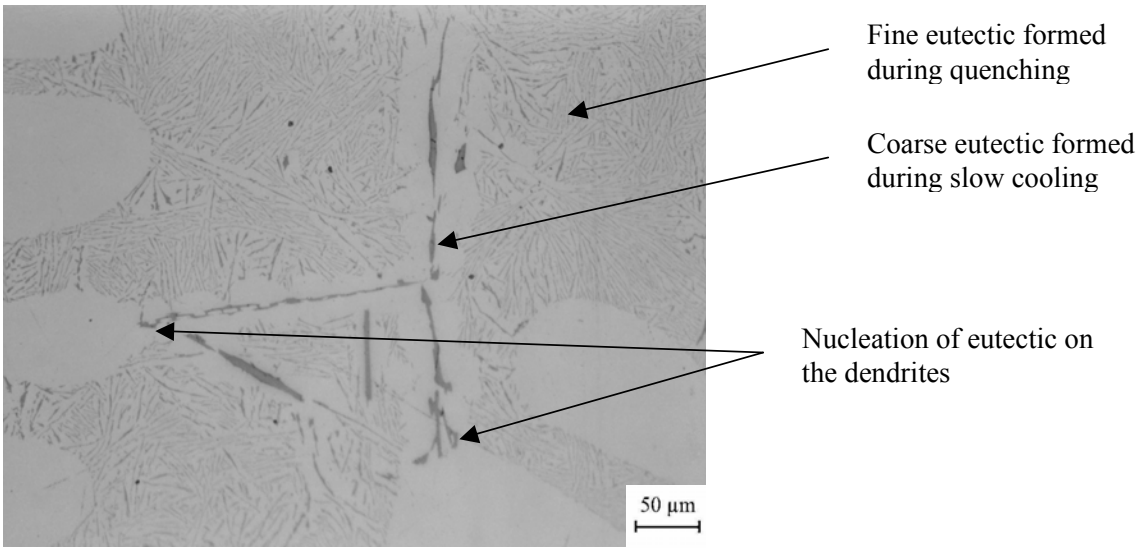

Figure 32: Optical micrograph of Al-6.74%Si quenched at 10% of the eutectic plateau. Polished with colloidal silica

Figure 33 shows another microstructure of quenched sample which reveals that eutectic silicon seems to be nucleating on the dendrite. The region of interest is enlarged in Figure 33 where a eutectic silicon needle (1) seems to grow out of a dendrite arm. The white curve in the enlarged section shows the boundary between this dendrite arm and the eutectic region. Region (3) is the aluminum in the eutectic. On close observation, the eutectic silicon needle (2) seems to be growing out of the aluminum in the eutectic. Hence, it seems that silicon in the eutectic could also nucleate on the aluminum in the eutectic. This observation could be easily overlooked if only orientation relationships were to be considered

without performing microstructure analysis. Because there is no orientation difference between aluminum in the eutectic and primary aluminum, [75-77] examining the orientation relationship between silicon in the eutectic and aluminum in the eutectic, or primary aluminum, does not necessarily reveal where the eutectic silicon is nucleating. Assuming silicon in the eutectic nucleates on the aluminum in the eutectic, orientation analysis would suggest that silicon in the eutectic has a unique orientation relationship with the primary aluminum or eutectic aluminum. Orientation analysis cannot exactly pinpoint whether eutectic silicon is nucleating on the eutectic aluminum or on the primary aluminum. However, the quench experiments conducted in this study gives direct evidence of eutectic silicon nucleating on eutectic aluminum.

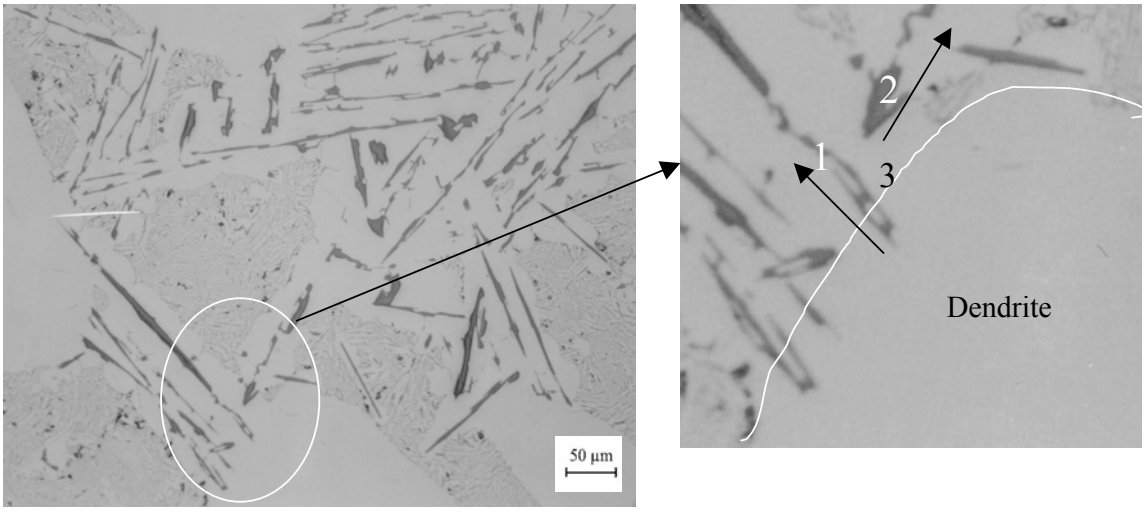

Figure 33: Optical micrograph of Al-6.74%Si quenched at 40% of the eutectic plateau. Polished with colloidal silica

Scanning electron microscopy of the quench samples was performed with electropolished samples, as samples polished with colloidal silica did not provide enough contrast. Figure 34 shows a SEM micrograph of Al-11.18%Si quenched at 10% of the eutectic plateau. Electropolishing etches the samples deeply by dissolving the aluminum layer in the samples, thus bringing out the features of the microstructure more clearly. Figure 34 shows the coarse eutectic silicon needles (white) and aluminum (grey). Eutectic aluminum nucleates on the silicon needles and grows in a direction perpendicular to the growth direction of needles. The hemispherical grains of eutectic aluminum are clearly seen in Figure 34.

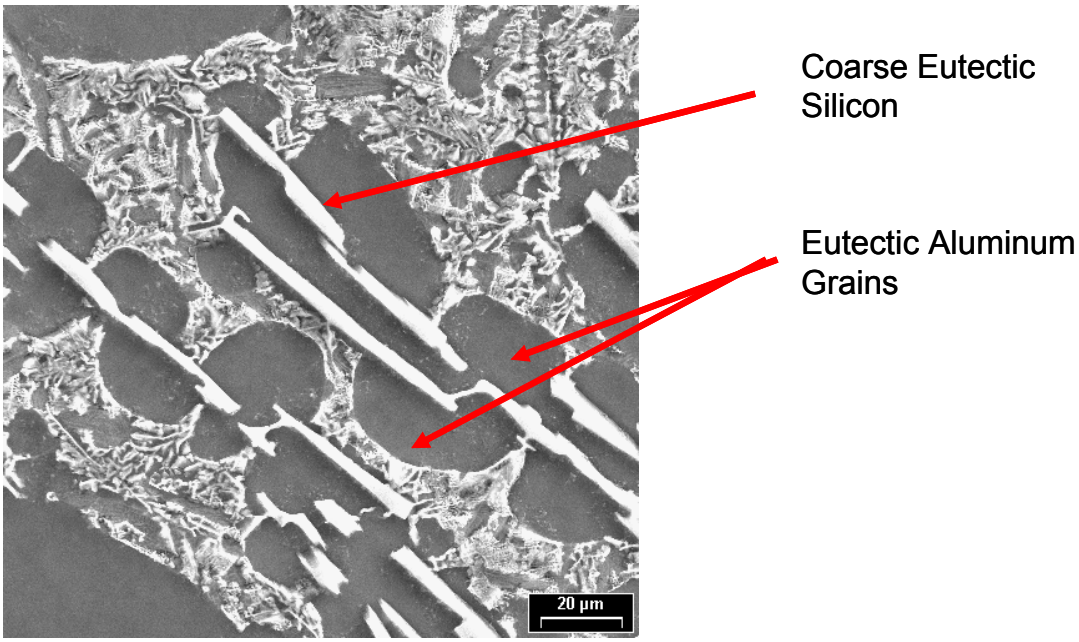

Figure 34: SEM micrograph of Al-11.18%Si quenched at 10% of the eutectic plateau.of alloy. Electropolished.

One more observation that can be made is multiple grains of eutectic aluminum seem to be nucleating on the silicon adjacent to each other. All these observations are explicable only if silicon were to grow ahead of the aluminum at the interface. Silicon seems to grow faster than aluminum in unmodified alloys. Thus growth of silicon increases the concentration of aluminum around itself. The slower growth rate of aluminum at the interface causes supersaturated aluminum around the silicon flakes which are ahead of the interface to nucleate on the silicon flake. Thus, renucleation of aluminum along the silicon flakes leads to the formation of multiple eutectic aluminum grains. Mcleod et al [65] predicted this phenomenon but they lacked the microstructural proof presented in this work. Mcleod [65] determined that quantity of silicon rejected by aluminum phase ($C_e(1-k)$) is very high for diffusion to dispose of the rejected silicon. Thus the rejected silicon acts as a barrier for growth of aluminum, effectively making aluminum to renucleate again and again on the silicon.

Previous figures showed whether eutectic nucleates on the primary aluminum or within the interdendritic melt. However, another mode of nucleation of eutectic is possible, which is nucleation and growth from the mold walls. Nucleation of eutectic from the mold walls is easier because of the heterogeneous nucleation sites available on the mold wall. Moreover, mold walls offer easy source of removing the heat released due to the solidification of eutectic. Figure 35 shows the nucleation and growth of eutectic silicon flakes from the mold walls in

unmodified alloys. Thus, nucleation of eutectic on mold walls is significant in unmodified alloys.

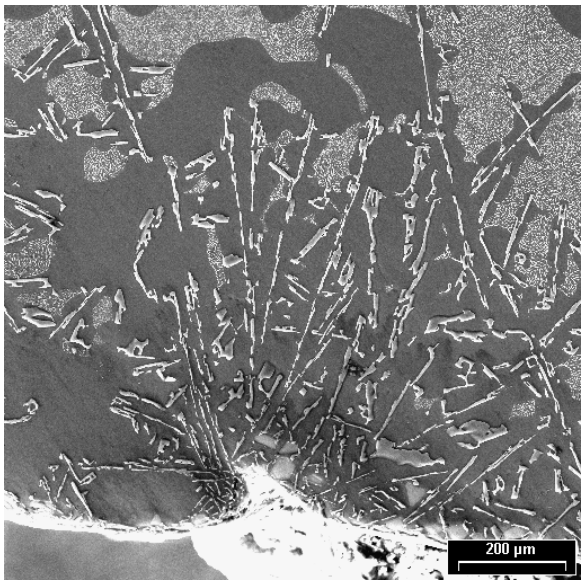

Figure 35: Growth of eutectic from the mold wall in Al-10.72%Si-0.0023%P alloy quenched at 10% of the eutectic plateau

However, observation of the macrostructure of the samples revealed that though nucleation of eutectic on the mold walls is significant, there is still some eutectic nucleating on the primary aluminum away from the wall. This phenomenon is clearly observed in Figure 36, which shows the macrostructure of a Al-6.74%Si alloy quenched at 40% of the eutectic plateau. Coarse eutectic as marked in Figure 36 shows the regions where eutectic nucleates upon the primary aluminum and away from the walls. Flood and Hunt, [78] who studied the macrostructure of aluminum silicon alloys, observed the same results as illustrated in this study.

Thus, in unmodified alloys, eutectic silicon nucleates on the primary aluminum and the mold walls. Eutectic aluminum nucleates on the growing eutectic silicon. Eutectic aluminum nucleates again and again on the same eutectic silicon forming multiple grains beside the growing silicon flakes.

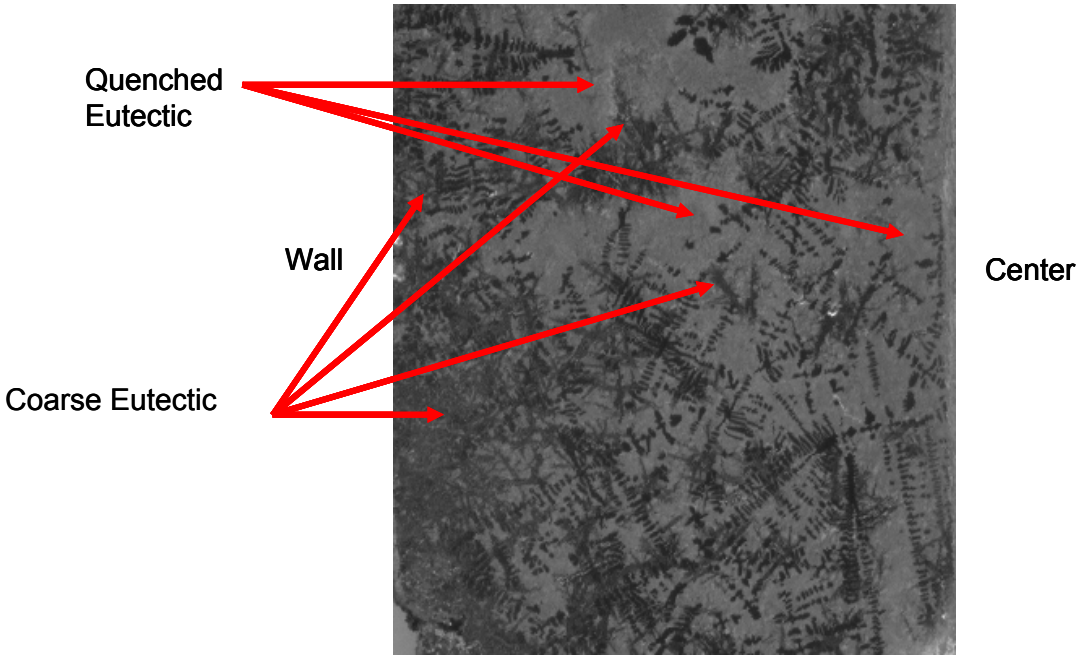

Figure 36: Macrostructure of Al-6.74%Si quenched at 40% of the eutectic plateau, showing growth of eutectic away from the growth front from the wall. Electropolished

Figure 37 shows the SEM micrograph of modified alloy without phosphorous. The silicon morphology is modified due to the addition of strontium from flakes to fibrous morphology. However, it is difficult to see where eutectic silicon seems to nucleate. In Figure 37, eutectic silicon seems to nucleate randomly within the interdendritic melt and not on the primary aluminum. Another important observation is that silicon does not nucleate ahead of the growing interface.

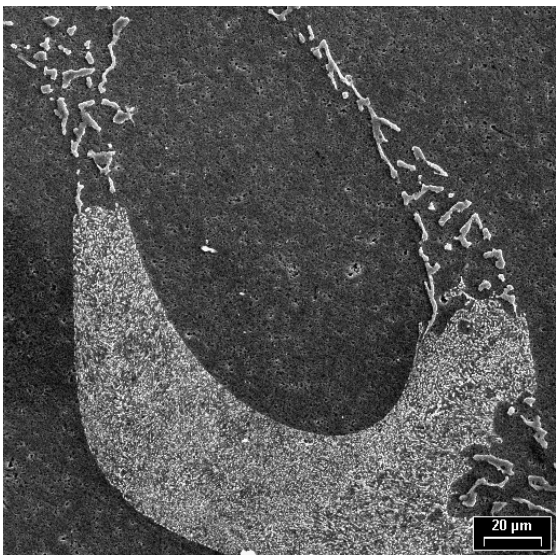

Figure 37: SEM micrograph of Al-6.6%Si-0.029%Sr quenched at 10% of the eutectic plateau.of alloy. Electropolished

However in some rare instances such as shown in Figure 38, eutectic silicon seems to nucleate and grow from the primary aluminum dendrites. Hence the question of nucleation of eutectic is still unclear and needs to be further analyzed.

Macrostructure of the modified alloy samples revealed that nucleation of eutectic on the mold walls is predominant. The nucleation on mold walls is clearly observed in Figure 39, which shows the macrostructure of a Al-6.6%Si-0.029%Sr alloy quenched at 10% of the eutectic plateau.

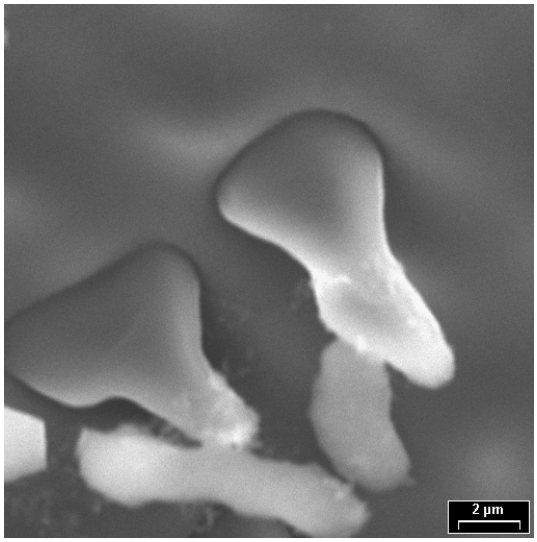

Figure 38: SEM micrograph of Al-6.6%Si-0.029%Sr quenched at 40% of the eutectic plateau.of alloy showing nucleation of eutectic silicon on primary aluminum. Electropolished

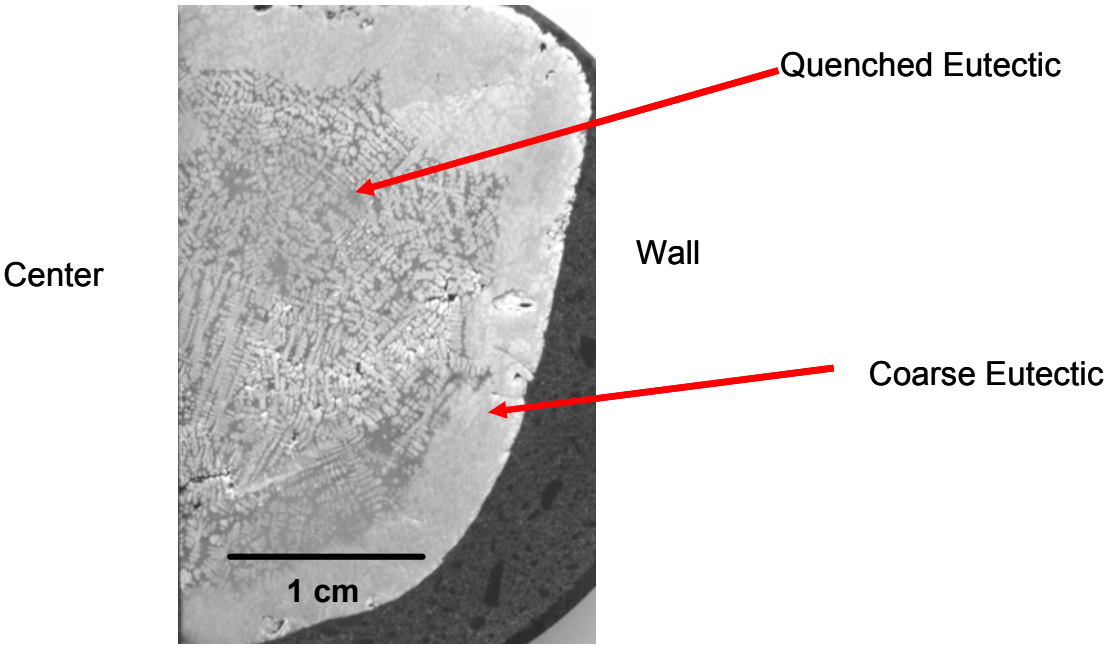

Figure 39: Macrostructure of Al-6.6%Si-0.029%Sr quenched at 10% of eutectic plateau

Figure 40 shows the macrostructure of a modified alloy close to the wall. Coarse eutectic is seen only close to the wall. Eutectic did not nucleate on the primary aluminum or within the interdendritic melt away from the eutectic growth front.

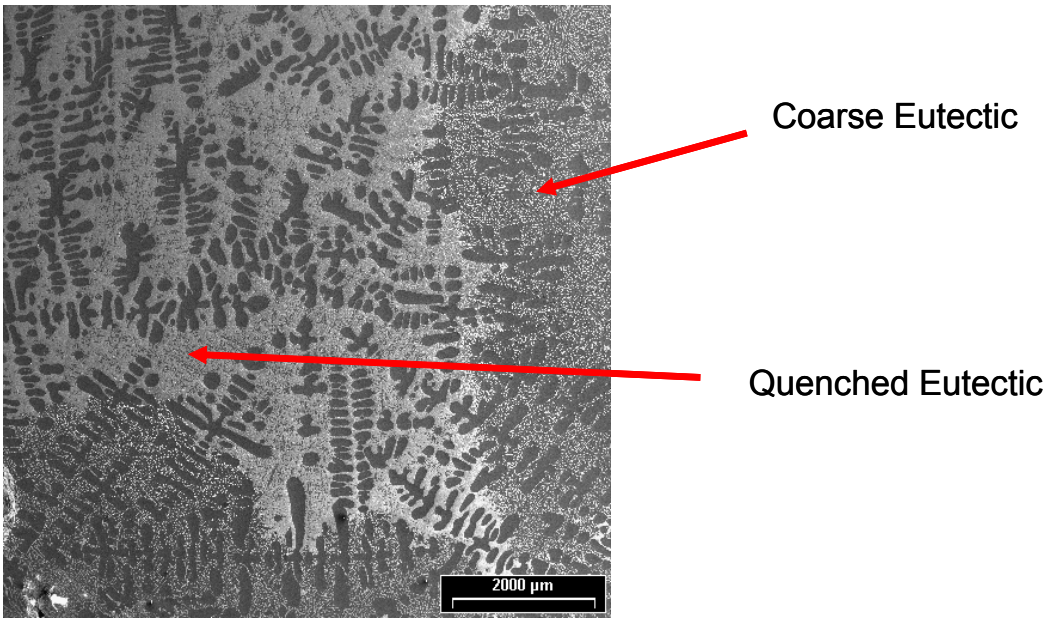

Figure 40: Macrostructure of Al-10.72%Si-0.023%Sr-0.0023%P quenched at 10% of the eutectic plateau

Results from previous investigations suggest that for strontium levels between 0 to 110 ppm, eutectic grains[4] nucleates independently within the interdendritic melt and at strontium levels 500 ppm and above eutectic nucleates on the primary aluminum. [79] However, if eutectic grains were to nucleate within the interdendritic melt and not from the walls or primary aluminum, the eutectic silicon/aluminum must nucleate ahead of the interface within the interdendritic

[4] Eutectic grains refers to both eutectic aluminum and eutectic silicon

melt. But there was no observed nucleation of eutectic silicon/aluminum ahead of the interface as clearly seen from Figure 40.

Thus, from the observations made thus far, primary aluminum acts as good nucleation site for eutectic in unmodified alloys than in modified alloys. This change in nucleation tendency of primary aluminum can be explained on the basis for change in surface energy brought about by the addition of modifiers in the melt. The results of sessile drop experiments as described in the following sections proves that surface energy change, alters the nucleation tendency in modified alloys.

4.1.3 Growth of Eutectic

In this section, the growth of eutectic in unmodified and modified alloys is presented. One of the important factors in understanding the growth phenomenon is the study of the 'leading phase' of eutectic, i.e if silicon or aluminum leads at the interface during growth. Hence, first the question of leading phase is addressed followed by the possible growth mechanism of eutectic especially the eutectic silicon is discussed.

The microstructure in Figure 41 gives compelling evidence of aluminum nucleating on silicon and growing in a direction perpendicular to the growth of silicon. The multiple grains of eutectic aluminum which have nucleated on the eutectic silicon have a growth direction perpendicular to the eutectic silicon. Eutectic aluminum unable to keep abreast with the fast growing eutectic silicon

nucleates again and again to grow in a direction perpendicular to the silicon.

From the above argument, silicon leads at the interface

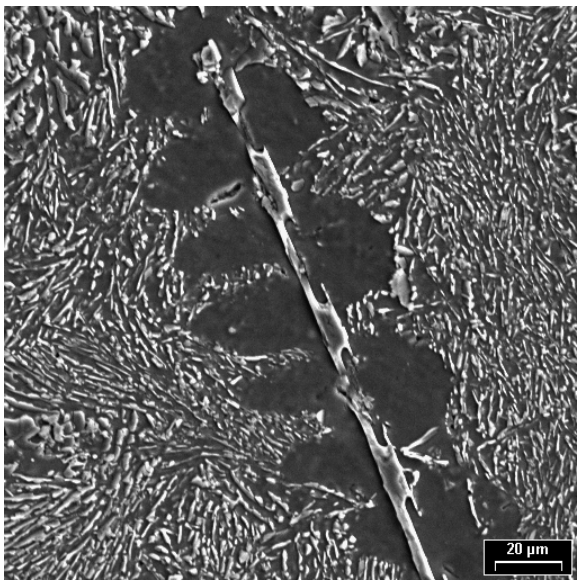

Figure 41: SEM micrograph of Al-10.72%Si 0.0023%P quenched at 10% of the eutectic plateau

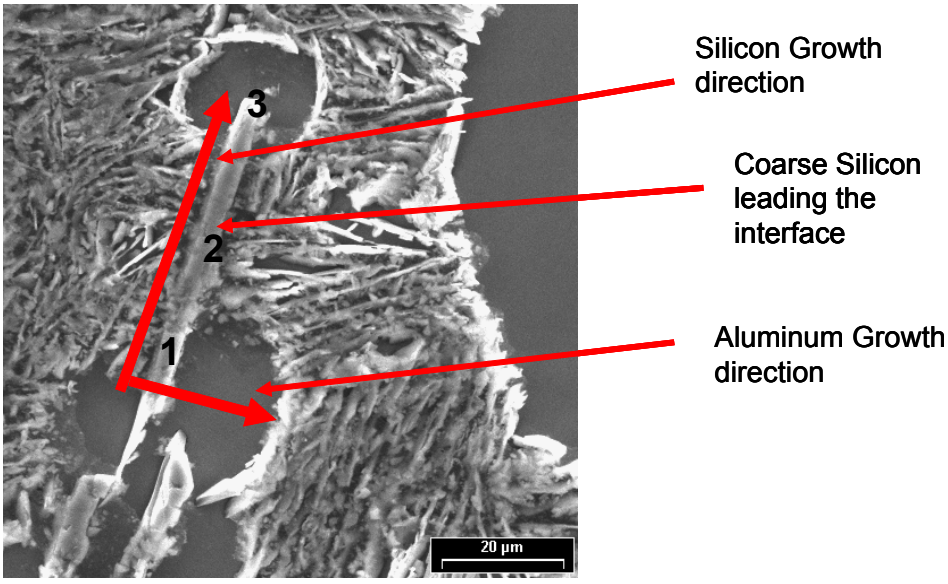

Figure 42: SEM micrograph of Al-6.52%Si-0.0019%P quenched at 10% of the eutectic plateau of alloy. Electropolished

Figure 42 reinforces the observations that silicon leads at the interface. In Figure 42 it can be seen that silicon grows in the direction 1→2→3. At region 1, the eutectic aluminum nucleates on silicon and grows in a perpendicular direction. At region 2 silicon leads at the interface and eutectic aluminum is unable to keep up with silicon. Again at region 3, eutectic aluminum nucleates on silicon. Aluminum which tends to surround silicon seems to be an artifact of quenching. During quenching heat is extracted suddenly and since aluminum has higher thermal conductivity and lower latent heat of solidification it tends to grow faster than silicon. [61] Silicon has been proved to be the leading phase in unmodified alloy. [15] Figure 43 which shows the macrostructure of a unmodified alloy shows the 'rugged' nature of the liquid solid interface. The rough nature of the interface is clearly an indication of silicon leading the interface.

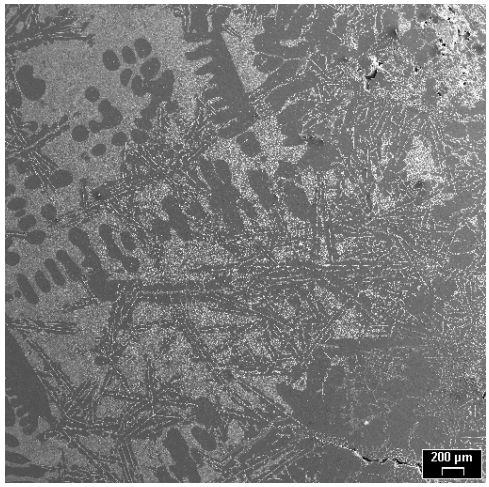

Figure 43: Macrostructure of Al-11.1%Si quenched at 10% of the eutectic plateau showing the rough solid liquid interface.

Growth mechanism of unmodified flake silicon, as reviewed in section 2 is still not completely understood. Growth of flake silicon is explained on the basis of various mechanisms including TPRE, [20] Layer growth mechanism [35] and a combination of TPRE and screw dislocations. [24] In this section, some of the microstructures illustrating the possible growth mechanisms are presented. However, it needs to be cautioned that the mechanisms presented here are by no means rigid and a further exhaustive study involving Transmission electron microscopy is suggested for complete understanding.

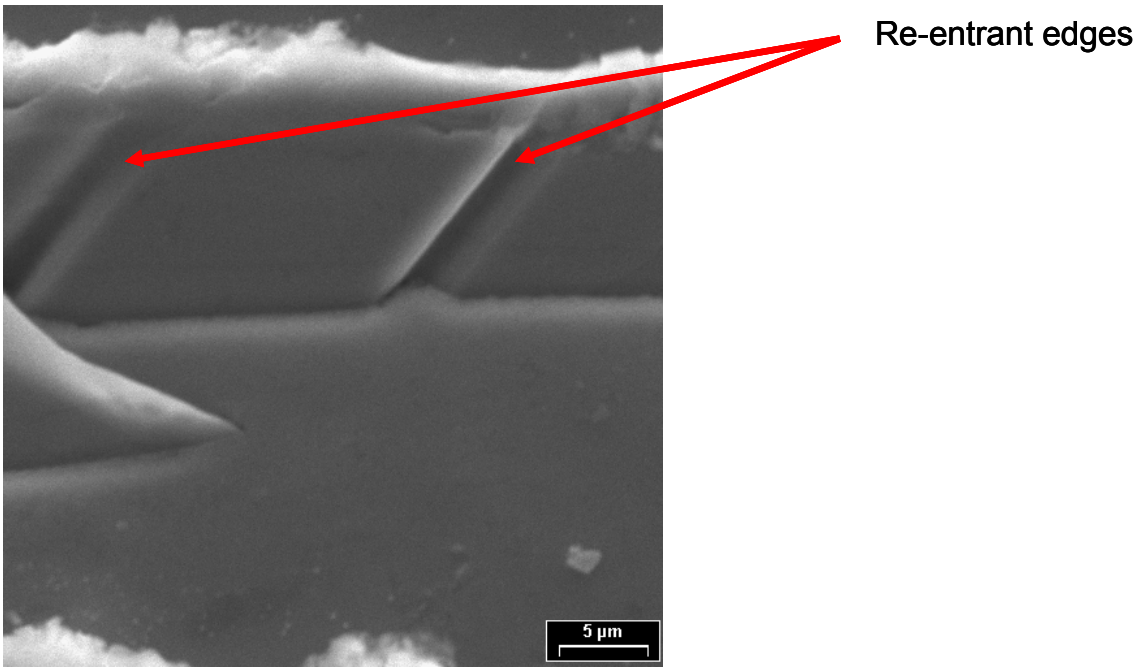

Figure 44: SEM micrograph showing possible Re-entrant edges in flake silicon

TPRE mechanism, which was first proposed by Hamilton [20] for growth of germanium dendrites, involves the formation of re-entrant edges at the tip of the silicon flake for growth. Figure 44 shows possible twin re-entrant edges

emerging at the tip of the silicon flake. Most of the flake silicon observed consisted of such re-entrant edges.

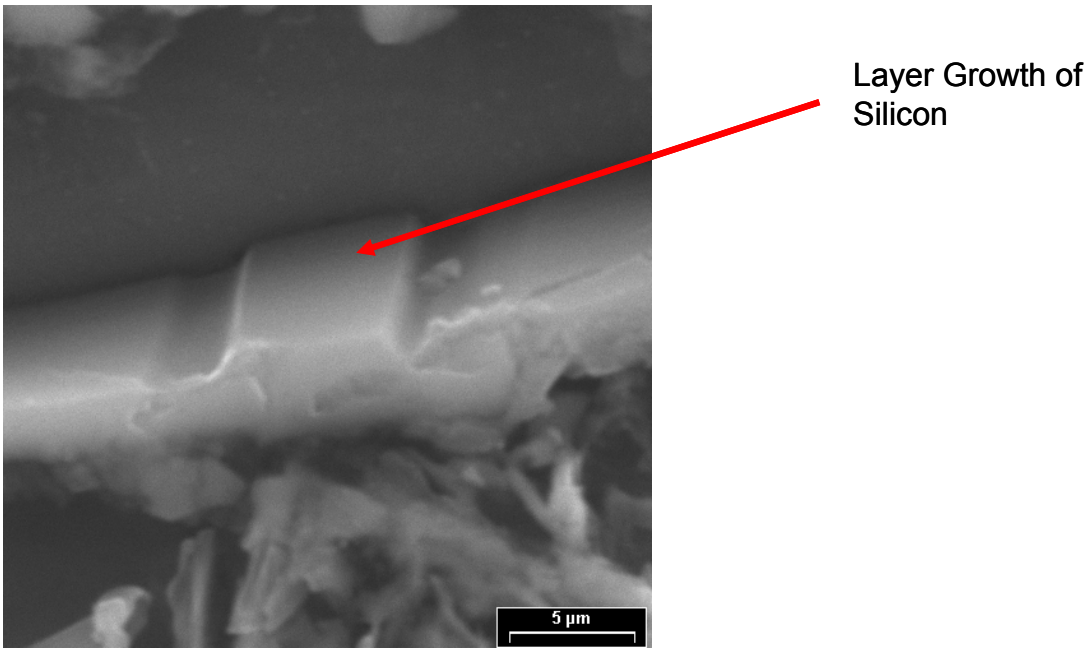

Figure 45: SEM micrograph showing flake silicon growing by layer mechanism

Layer growth mechanism, was proposed to be the predominant growth mechanism for growth of flake silicon by Hellawell et al. [35,45] For growth by layer mechanism to take place, surface nucleation is required. The surface nucleation can be initiated by formation of a silicon disk or by surface defects such as screw dislocations. Figure 45 shows a silicon flake growing by layer mechanism, in which surface nucleation has taken place. Figure 46 shows the possibility of a screw dislocation acting as a surface nucleation for layer growth mechanism. The contour shown on the left side of the figure resembles a growth by spiral mechanism, in which silicon atoms attach themselves to the surface

opening of a screw dislocation. Growth in such a case takes place in a spiral direction until, the tension generated in the loop stops further growth (Refer to the schematic in Figure 46).

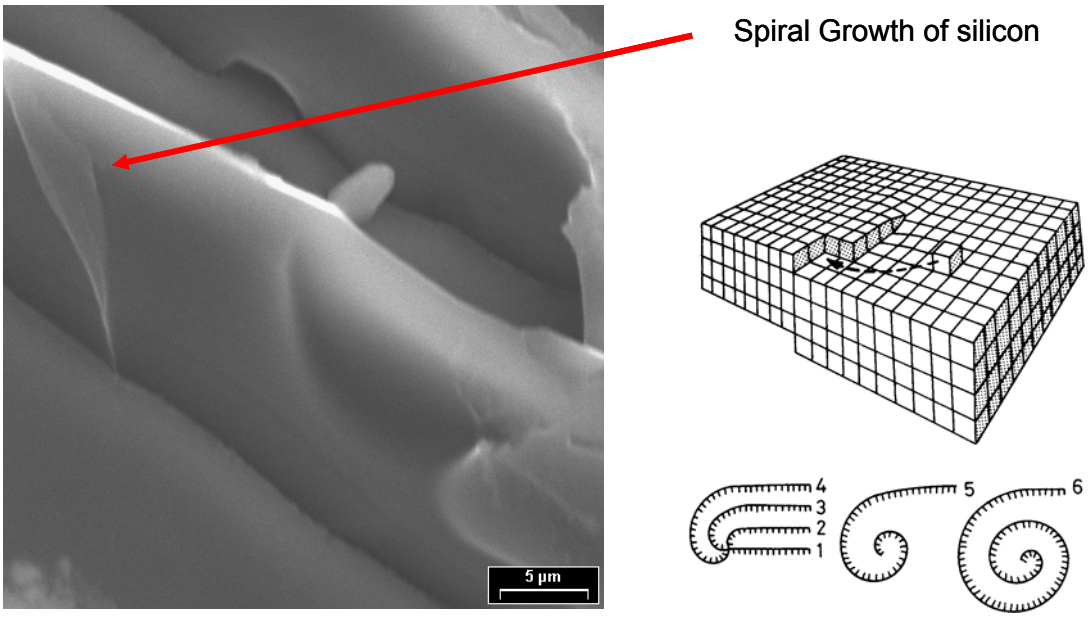

Figure 46: SEM micrograph showing possible spiral growth due to a screw dislocation

The role of screw dislocations in surface nucleation has not been given as much importance as re-entrant edges in the study of flake silicon growth. The difficulty in assessing the role of screw dislocations in growth phenomena is one of the main stumbling blocks in this respect. Thus the contour shown in Figure 46 cannot be confirmed to be a result of surface nucleation due to screw dislocation, but that is best hypothesis presently available in the literature to explain it.

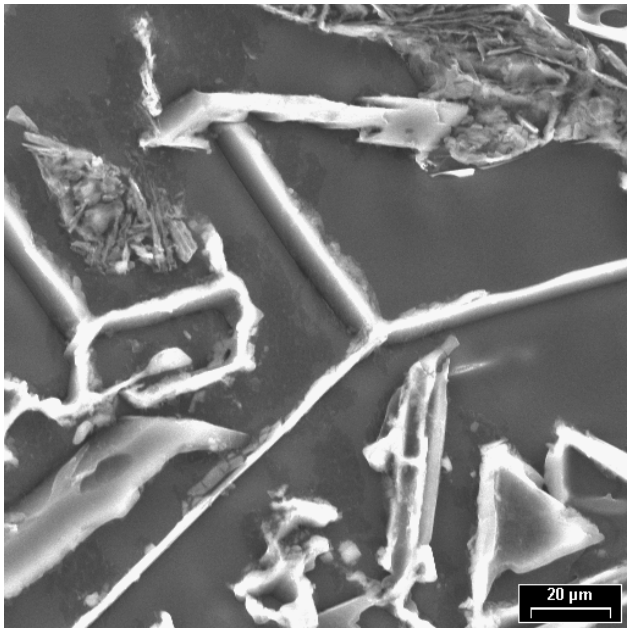

Figure 47: SEM micrograph of angular silicon observed in unmodified alloys

Apart from the flake silicon, some regions of unmodified samples also exhibited the characteristic angular silicon morphology observed in Region B of Figure 4. An approximate calculation of interface velocity was obtained by measuring the distance of eutectic growth front from the wall from the microstructure and dividing it by the time spent at the eutectic plateau obtained from cooling curve. An approximate interface velocity of 2.86µm/s was obtained. Since the cooling rate is known from thermal analysis, the corresponding temperature gradient in the melt can be calculated from the relationship.

Cooling rate = Temperature Gradient * Interface velocity

The resulting temperature gradient was calculated to be 1.7K/mm. The corresponding point in Figure 4 lays in the region B + C. Thus, the quenching experiment conducted is equivalent to directional solidification in region B+C. This explains the observations of angular silicon being formed in certain regions of the unmodified sample.

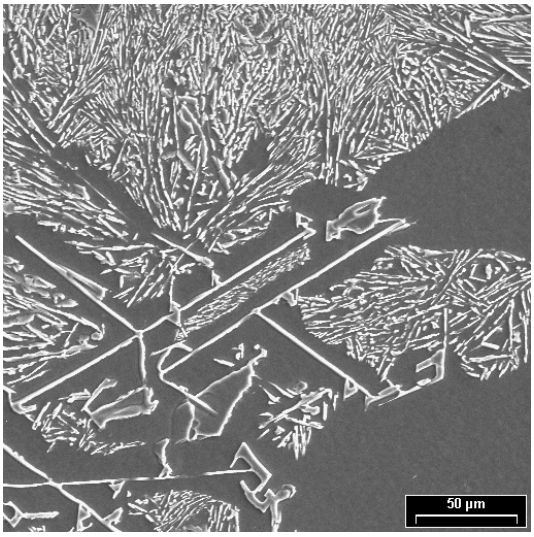

Figure 48: SEM micrograph of angular silicon with flake silicon in between them observed in unmodified alloys.

Figure 49 shows an SEM micrograph of a modified alloy. Aluminum is the leading phase in the modified alloy as seen clearly in Figure 49. Because of the lead of aluminum phase in modified alloys, the solid liquid interface is smooth as can be seen in Figure 40. In modified alloys, the silicon particles are finer than in unmodified alloys, which made it almost impossible to study the growth features using SEM. Hence other experiments were designed to further understand the effect of modifiers on the morphology of silicon. Study of the analogous Al-Ge system and sessile drop experiments for surface energy determinations are

some of the steps in this direction. Hence the results of these experiments are presented before a plausible explanation for growth of fibrous silicon upon addition of modifiers is proposed.

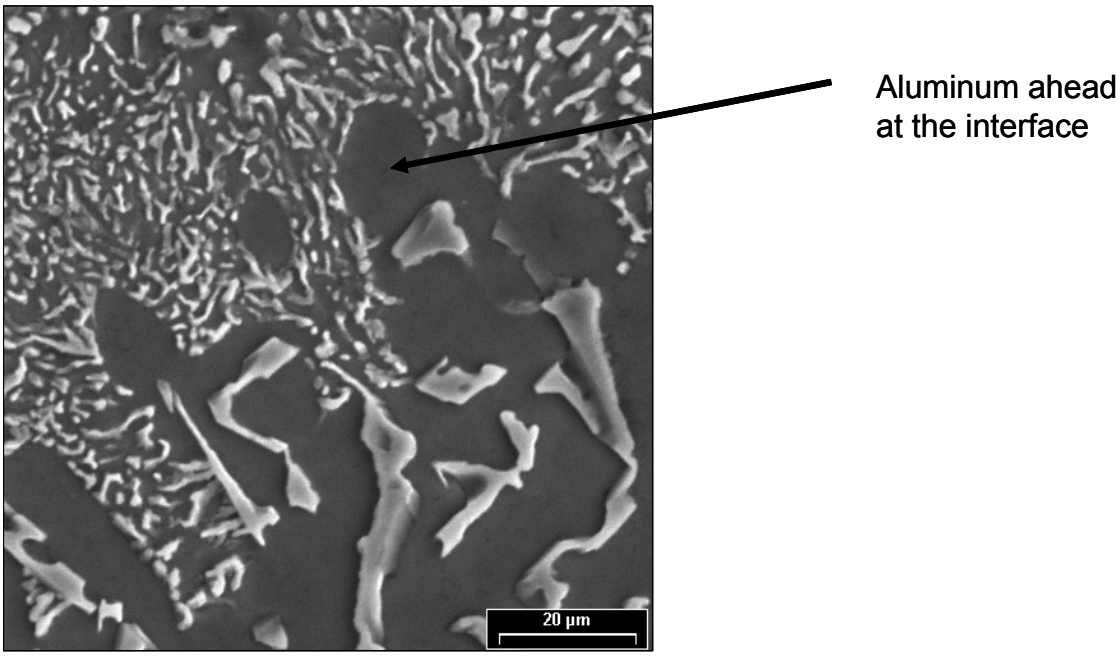

Figure 49: SEM micrograph of Al-10.4% Si-0.03%Sr quenched at 10% of the eutectic plateau

4.2 Sessile Drop Experiments

Results obtained from the unmodified and strontium modified eutectic droplets on the Al-1%Si substrate are listed in Table VII. Figure 50 shows sessile drops of the unmodified eutectic on the left and the modified eutectic on the right. In this Figure, the unmodified droplet had already completely wetted the Al-1%Si substrate, while the Sr modified droplet was still intact. Considering the results tabulated in Table VII, it was observed that the contact angles of the unmodified

and the Sr modified eutectic are different. The Sr modified eutectic droplet is comparatively less wetting than the unmodified droplet, as its contact angle is greater than that of the unmodified eutectic. Wetting time is the time between the incipient melting of the cubic pellet and when the pellet is completely flat on the substrate. Wetting time gives an indication of the ease with which the eutectic can flow over the substrate. Wetting time of an unmodified eutectic was found to be less than that of the Sr modified eutectic. The ability of a melt to wet the surface can be gauged by comparing the driving force for wetting. Table VII shows that the unmodified eutectic has over a magnitude more driving force for wetting than the strontium modified eutectic. Thus, an unmodified eutectic melt trying to fill the unfilled zones between the interdendritic networks would be able to flows easier on the dendrites than a Sr modified eutectic, resulting in impaired feedability and a wider distribution of pores in modified castings.

Table VII: Results of unmodified and Sr modified eutectic on Al-1%Si substrate at 577 °C

Parameter	Unmodified	Modified
Contact Angle	**129.5°**	**150°**
Wetting time (mins)	**19**	**30**
Driving force to wet (N)	**-85.32**	**-164.9**

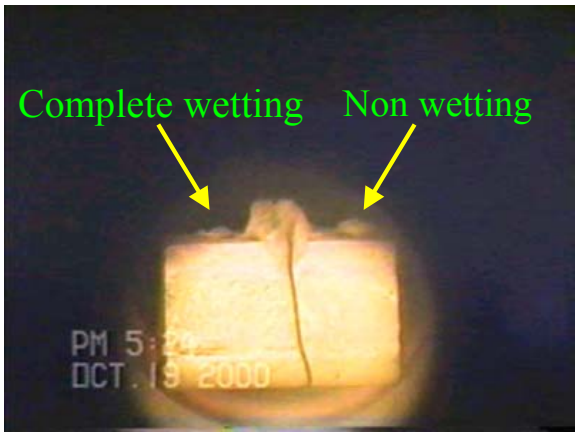

Figure 50: Sessile drops of completely wetted unmodified eutectic and Sr modified eutectic

Previous work [11,42,62,80,81] on interfacial energies of Al-Si alloys used only ceramic substrates. Hence it is difficult to correlate the results obtained in this study with them. Emadi et al [42] studied the interfacial energies and volumetric shrinkage of A356 alloy with sodium and strontium addition on an alumina substrate in a high purity argon atmosphere. Their results show that addition of modifiers like sodium and strontium reduces the liquid vapor (argon) interfacial energy. The obtained values of interfacial energies were used in the calculation of the pore size created by entrapment of hydrogen gas. The resulting pore sizes were further correlated to the radius of the flow channels in the interdendritic network. However, the experiments used an argon atmosphere and not a hydrogen atmosphere. Thus, the authors made an implicit assumption that interfacial energy of liquid/vapor (argon) is the same as the interfacial energy of liquid/vapor (hydrogen), which need not be the case.

In order to understand the implications of surface energies on the nucleation of the eutectic on primary aluminum, the following mathematical analysis was performed. In an actual casting, the droplet appears as in Figure 51a, in which the eutectic solidifies on a heterogeneous nucleant, M. The surface energies acting are γ_{SL}, $\gamma_{ML}$and γ_{SM}.

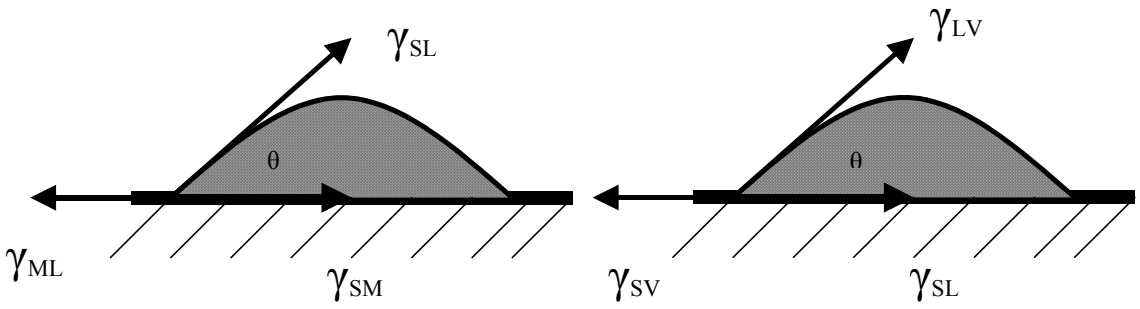

Figure 51: Schematic of eutectic solidification in a) actual casting b) sessile drop

However, in a sessile drop, the surface energies are different from that of an actual casting. The directions in which they are oriented are also different. (Figure 51b).The common point in the two cases is the wetting angle. For any heterogeneous nucleation, the basic governing equation is given by [13]

$$\Delta G_{het} = \left\{ -\frac{4}{3}\pi r^3 \Delta G_V + 4\pi r^2 \gamma_{SL} \right\} S(\theta) \qquad (5)$$

where

$$S(\theta) = (2 + Cos\,\theta)(1 - Cos\,\theta)^2 / 4 \quad (6)$$

From Table VII, it is observed that the contact angle of the modified eutectic droplet is larger than that of the unmodified eutectic. Thus, the value of S(θ) is higher for the Sr modified eutectic than for the unmodified eutectic. Hence, the value of ΔG_{het} for an unmodified eutectic is lower than that of its modified counterpart. Accordingly, primary aluminum acts as a better heterogeneous nucleant for the unmodified eutectic than for the Sr modified eutectic (See section 4.1.2). This difference can lead to nucleation of eutectic in modified melts within the interdendritic liquid and not on the primary aluminum. Dahle et al [79] studied the effect of strontium content on nucleation of the eutectic, using EBSD techniques and quench experiments. Their results indicate that at strontium contents of 0.02%, the eutectic nucleates heterogeneously within the interdendritic melt and not on the primary aluminum agreeing with the observations made in this study.

4.3 Study of Analogous System: Al-Ge System

Figure 52 shows the microstructures of Al-7Si and Al-20Ge without the addition of any modifiers. Germanium in the Al-Ge eutectic (Figure. 52b) is different from the eutectic silicon morphology (Figure. 30(a)). Unlike eutectic silicon, which exists in the form of sharp needles, germanium in the eutectic does not have

sharp faceted morphology. In some of the regions, germanium seems to have grown in the form of fibers as in modified silicon. It is known that both germanium and silicon normally grow by twin plane re-entrant edge mechanism (TPRE). [20] In a pure Al-Ge system without any modifiers germanium evolves in the form of fibers at normal cooling rates. This can be explained on the basis of interfacial energy. Germanium is strongly anisotropic like silicon and the fraction of β phase at eutectic composition in Al-Ge system is 0.28. It is known that interface area of fibers is lower than that for lamellae at volume fractions which are smaller than about 0.3. [2] Since eutectic volume fraction in Al-Ge system is close to 0.3, we observe both lamellae and fibrous morphology. Here, the strong anisotropy of growth of germanium and its interface energy plays an important role.

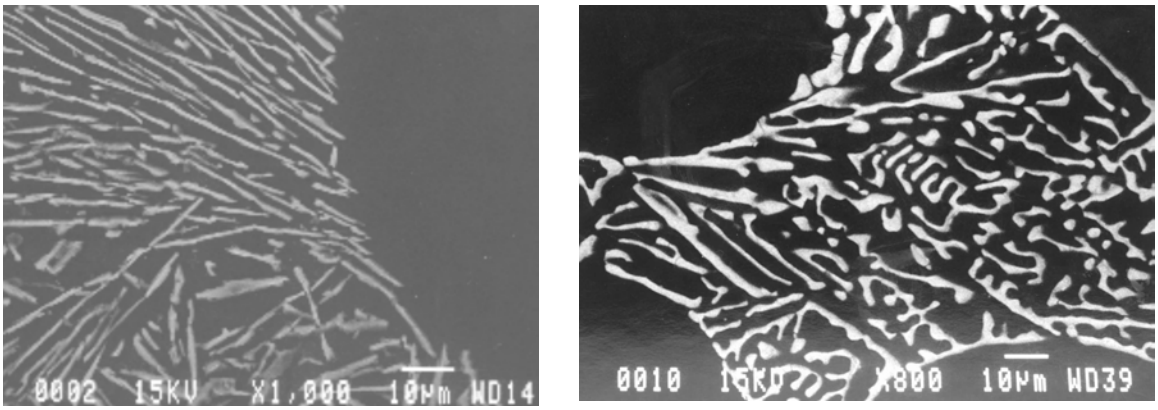

Figure 52: SEM micrographs of (a) Unmodified Al-7%Si (b) unmodified Al-20%Ge

Figure 53 shows the morphology of Al-Ge alloy on the addition of strontium. Comparing Figures 52(b) and 53, it can be observed that Sr modifies the Al-Ge eutectic. The Al-Ge eutectic becomes much finer than the eutectic in Al-Si alloys.

The modified eutectic cannot be resolved unless it has been magnified 10,000 times.

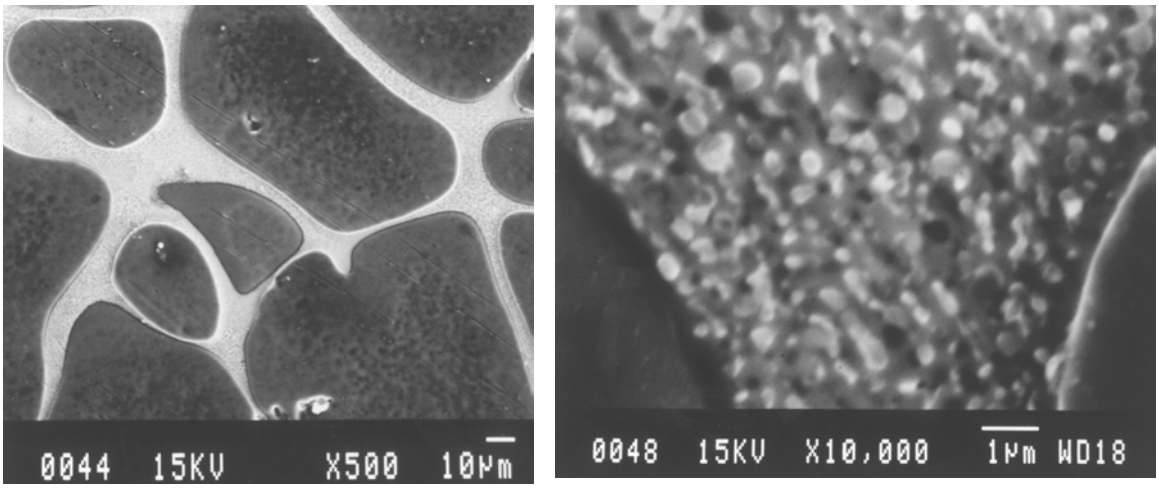

(a) (b)

Figure 53: SEM Micrographs of Sr modified Al-20Ge alloy.

Germanium in the eutectic upon modification with strontium forms a spherical particulate structure. When the interfacial energy is very high, the eutectic phase tries to assume morphology with minimum surface area resulting in spherical structure. [13] The cooling curves of both alloys are showed in figure 32. Upon addition of Sr the under-cooling in the Al-Ge alloy increases, as in Al-Si system.

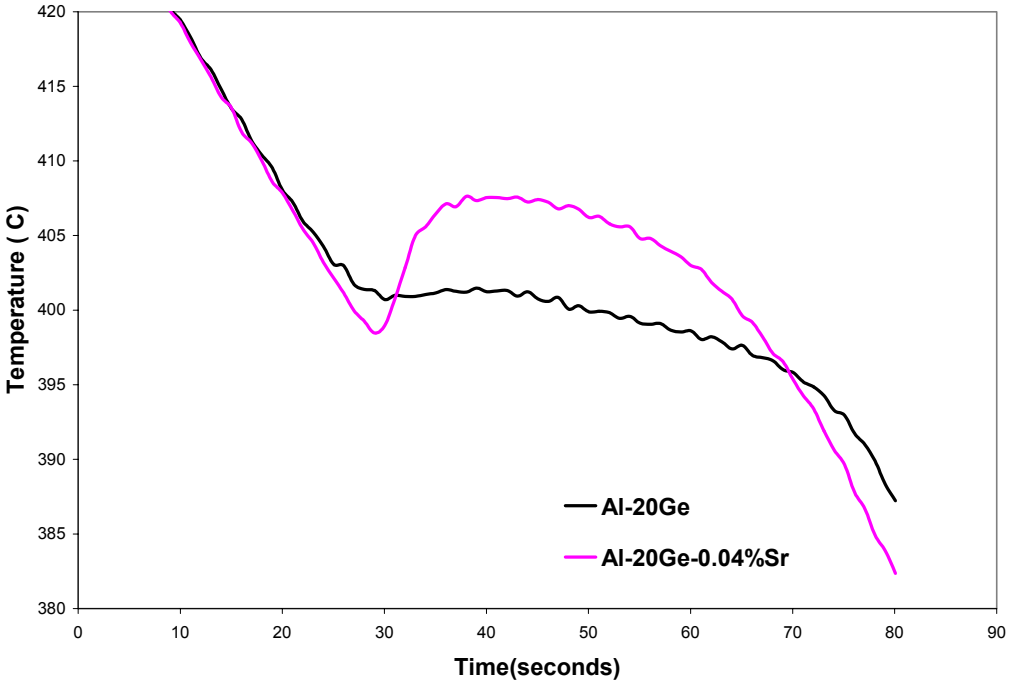

Figure 54: Cooling curves of unmodified and Sr modified Al-Ge alloy

Growth of Fibrous Silicon

With the results of sessile drop experiments and Al-Ge experiments in perspective, a possible explanation of the growth of fibrous silicon upon addition of modifiers is presented in this section.

From quench experiments, it was observed that aluminum is the leading phase at the solid liquid interface in Strontium modified alloys. This lead of aluminum over silicon as compared to silicon over aluminum in unmodified alloys causes the change in the morphology of silicon. When aluminum leads at the solid liquid interface, it grows into the liquid which is essentially super cooled for its solidification. This supercooled liquid ahead of the interface causes constitutional under-cooling, making aluminum essentially grow In the form of

dendrites. However, the interceding silicon phase does not allow complete dendrite morphology in eutectic aluminum phase. As soon as secondary dendrites start growing out, the silicon phase reaches the eutectic aluminum, thus preventing complete dendrite morphology in eutectic aluminum. The aluminum growing ahead of the silicon imposes a restriction on the space in which silicon can grow. Essentially silicon has to occupy the 'negative' space of aluminum, i.e the region left unoccupied by aluminum. This 'negative space' of partial dendrite morphology results in the form of a fibrous silicon. Moreover, the suppression of nucleation of silicon by strontium causes the silicon to grow continuously in the form of fibers.

The change in lead at the interface from silicon to aluminum is due to the altered surface energies by addition of modifiers, as proposed by Thall and Chalmers. [61] Further evidence of the importance of surface energies in determining the morphology of silicon comes from the Al-Ge experiments. In Al-Ge system, it was seen that even without addition of modifiers the morphology of germanium is semi-fibrous or non-flaky structure.

Another evidence of the role of surface energy in altering the morphology of silicon is available from the sessile drop experiment. It was shown previously, that in sessile drop experiments both modified and unmodified sessile drops completely wet the surface of the substrate after sufficient time. Unmodified alloys wet the surface easily and modified alloys take a longer time to wet the

surface. But once wetting takes place, the effect of difference in surface energies is lost. Thus, if sufficient time were to be given for a modified alloy to solidify so to lose the effect of surface energy, the resulting morphology of silicon should be flaky.

Figure 55 shows the SEM micrograph of a aluminum silicon with strontium. The silicon is not fibrous inspite of the presence of strontium in the melt. The slow cooling of the alloy during eutectic plateau was sufficient to remove the effect of strontium on the surface tension, thus resulting in the formation of flake silicon. It is worth mentioning that multiple samples showed flake silicon inspite of the presence of strontium. The modifier content was analyzed by a spectrometer after quenching to make sure the modifier was present in the alloy.

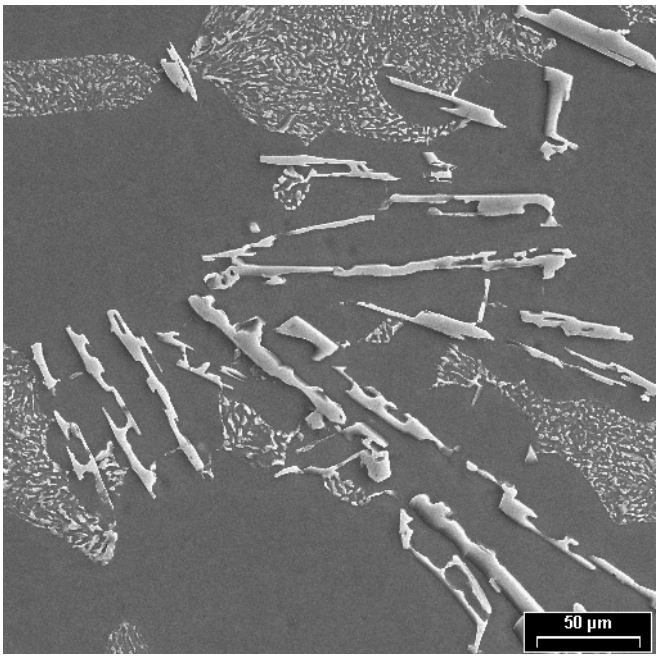

Figure 55: Flake Silicon in Al-10.4%Si-0.03%Sr quenched at 40% of the eutectic plateau

4.4 Study of Strontium Addition on Hydrogen Content

The results of hydrogen measurements for 319 and 380 alloys for various levels of strontium addition are shown in figures 56 and 57. Since the experiments were conducted on different days, the absolute content of hydrogen in each of the experiment was different.

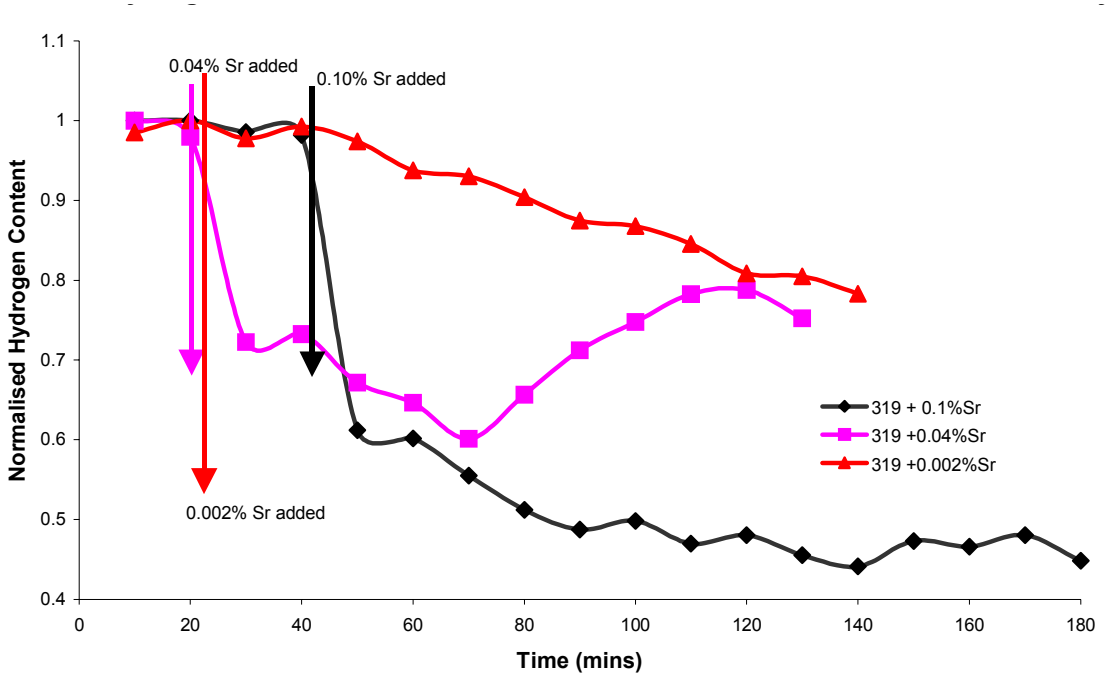

Figure 56: Hydrogen content versus time for three different strontium levels in 319 alloy

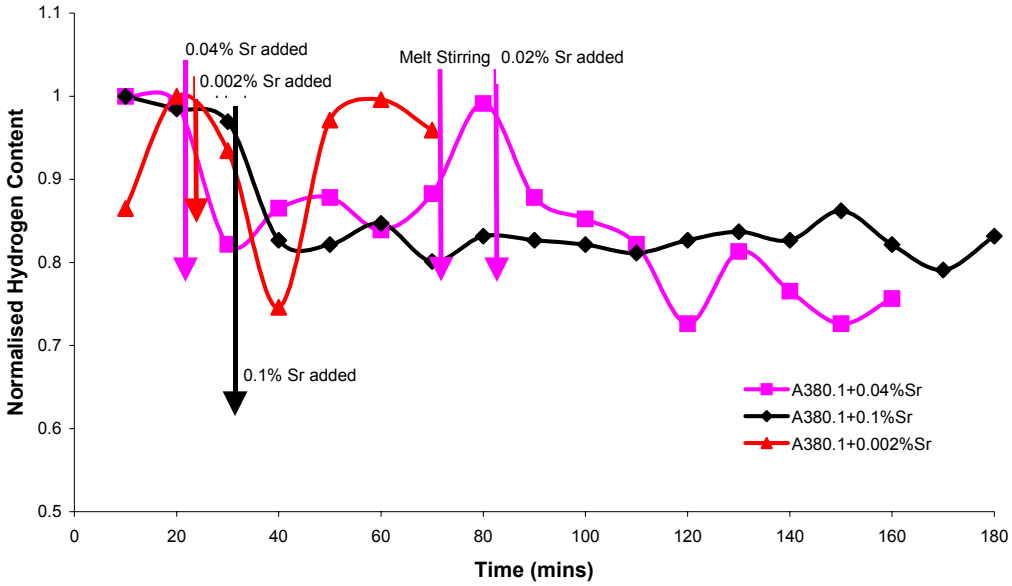

Figure 57: Hydrogen content versus time for three different strontium levels in 380 alloy

Results were compared by normalizing the hydrogen content at any instant to the maximum hydrogen content of a particular experiment. From the graphs, it can be seen that addition of strontium leads to a drop in hydrogen content of the melt. It was observed that the drop in hydrogen content increased with the amount of strontium added. When the strontium content added was less (0.002% and 0.04%) re-gassing of melt takes place, causing the hydrogen content to revert back to its initial level. On addition of high amounts of strontium (0.1%) the drop in hydrogen content was retained for longer periods of time.

Microstructures of the samples collected were analyzed to look for correlation between modification and hydrogen content. The microstructures are shown in Figure 58. Addition of 0.002%Sr, showed a drop in hydrogen content, but did not

modify the microstructure. Thus, drop in hydrogen content due to modifier addition has no relation with modification.

Denton and Spittle [41] studied the effects of addition of 0.04wt% Sr on the hydrogen content in LM6 melts. Hydrogen concentration in the melt was measured using a SEVERN science ‘Hysan’ Hydrogen in Aluminum Analyzer. Severn test is a variation of the basic Reduced Pressure Test (RPT). The results from the experiments indicated that the presence of strontium leads to increased hydrogen pick up. However, Hysan method of hydrogen measurements has several shortcomings. This test actually reveals the combined affect of hydrogen and inclusions. [82,83] Experiments have shown that the same heat of melt behaved differently before and after filtration. In the filtered melt much less porosity was produced than in the unfiltered melt. Moreover, Gauge Repeatability and Reproducibility Analysis(R&R) conducted by Lastowski & Makhlouf [84,85] on the RPT test indicated that there is a high degree of variability in the RPT results obtained.

319 Alloy **380 Alloy**

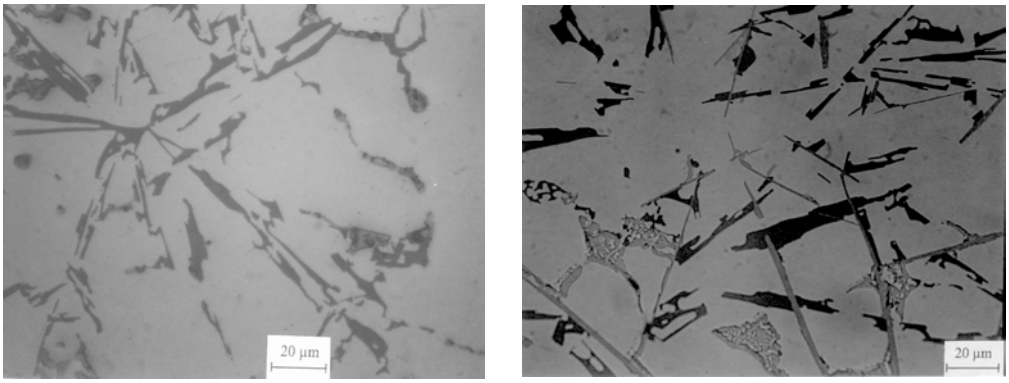

0.002%Sr

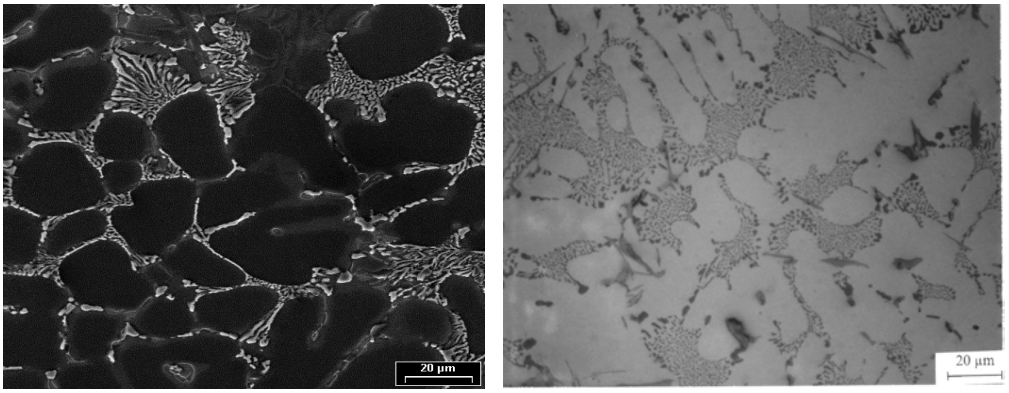

0.04%Sr

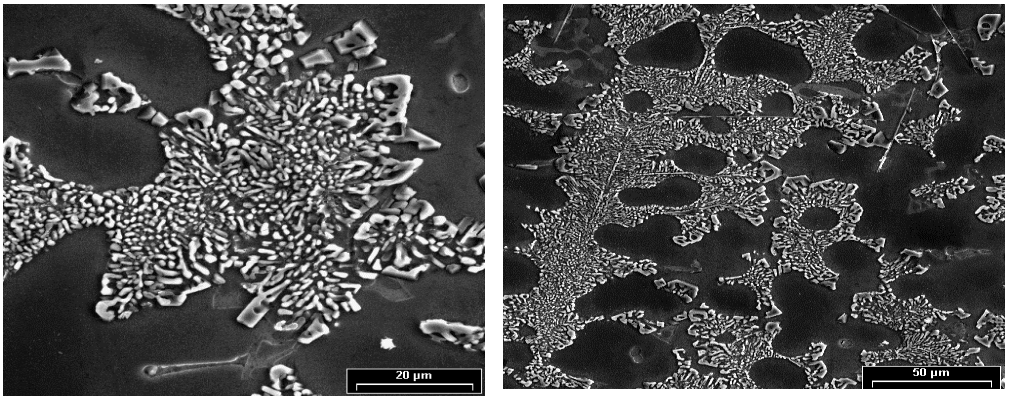

0.1%Sr

Figure 58: Microstructures of 319 and 380 alloys with three different levels of modification.

Gruzleski et al [72] used Telegas™ to measure hydrogen content in Sr modified 356 melts. Telegas™ operates on the same principle as Alscan™. They observed no change in the hydrogen content on addition of strontium. However in their experiments, hydrogen content was not continuously monitored throughout the experiments. The hydrogen content was not measured until after 30 minutes after the addition of strontium. In our experiments, there was significant drop in the hydrogen content within 30 minutes after the addition of Al-10%Sr master alloy. Moreover, the experiments in this study were conducted with Alscan™, which had a better probe and more accurate compositional factors than Telegas™.

The drop in hydrogen content on strontium addition could be because of the formation of strontium hydrides. The stable hydride of strontium is SrH_2. Plot of free energy of formation of strontium hydride versus temperature is shown in Figure 59. At 700°C the free energy of formation of SrH_2 is negative. Thus, thermodynamically, formation of strontium hydride is feasible. The free energy of formation of sodium hydride is positive at 700°C. If hydrogen content of the melt was decreasing due to the formation of strontium hydrides, addition of sodium should not reduce the hydrogen content in the melt, as it cannot form sodium hydride. To investigate this, hydrogen content of a 319 melt was measured upon addition of sodium. The results are shown in Figure 60.

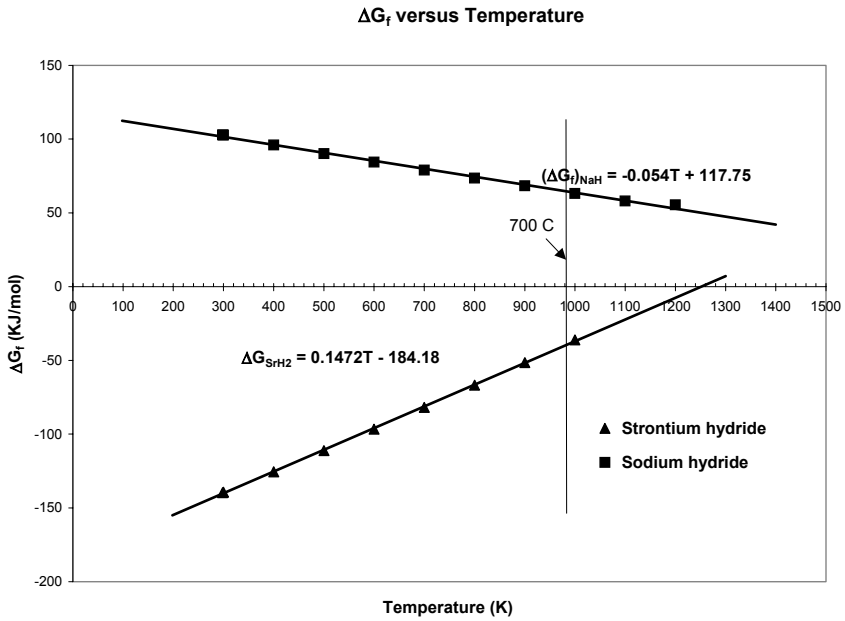

Figure 59: Free energy of formation of metal sodium hydride versus temperature.

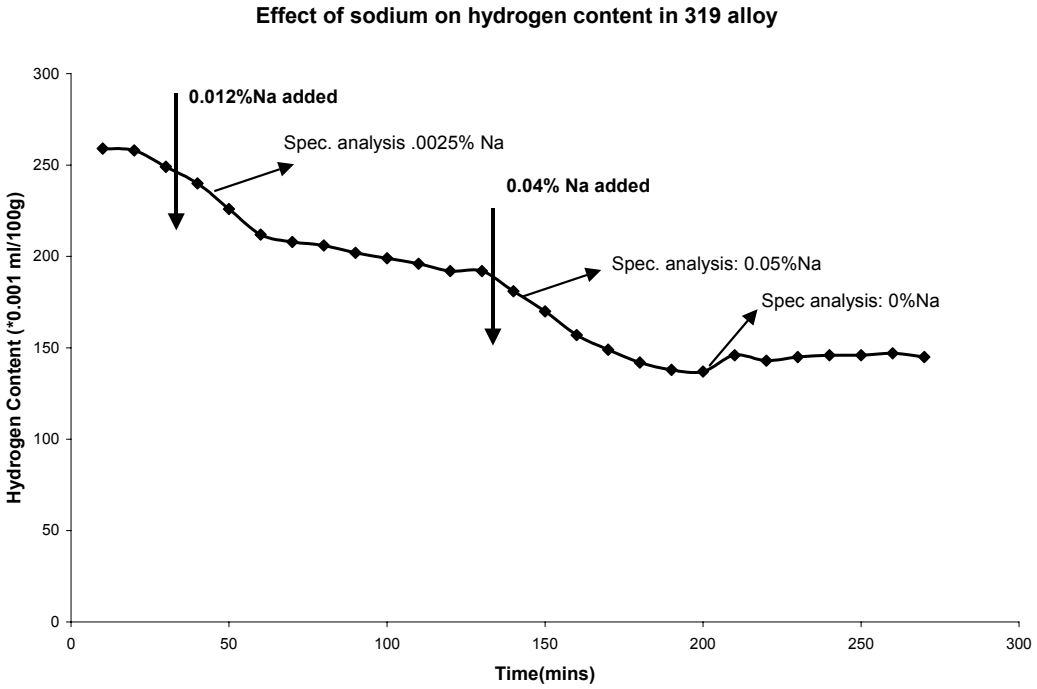

Figure 60: Hydrogen content on addition of metallic sodium in 319 alloy

Addition of sodium also resulted in drop in hydrogen content. But in the case of sodium the drop was gradual and not as sudden as strontium. Periodic samples were taken out to correlate the hydrogen content with the presence of sodium in the melt because of rapid fading of sodium. The gradual drop in hydrogen content was observed only till sodium was present in the melt. After the fading of sodium, the hydrogen content seemed to stabilize. This observation suggests that metal hydrides may not be responsible for drop in hydrogen content of the melt. It could be possible that the free energy of formation of sodium hydride is negative when sodium is present in liquid aluminum.

The observed changes can be easily explained on the basis of change in liquid surface energy upon addition of sodium or strontium. σ_{gL} is known to decrease upon addition of modifiers such as sodium or strontium. Consider the gas bubble nucleation equation:

$$P_g = P_o + \rho_L g_r h + \frac{2\sigma_{gL}}{r} \qquad (7)$$

where P_g is the total gas pressure in the bubble, P_o is the ambient pressure, $\rho_L g_r h$ constitutes the metallostatic pressure head and the final term is the pressure in the bubble resulting from the bubble-melt interfacial energy σ_{gL}. For a constant total gas pressure P_g, if the interfacial energy σ_{gL} decreases the radius of the bubble required to form a stable bubble also decreases. Thus, a decrease in interfacial energy would mean easier bubble nucleation. Easier

bubble nucleation would mean easy escape route for the gas to form bubble and escape. Thus addition of modifiers would lead to a decrease in the hydrogen content of the melt as observed in the results presented thus far. The reduced size of gas bubbles also explains the why modified melts contain fine pores as compared to coarser pores in unmodified alloys.

Appendix A

The surface tension of a liquid is defined as the measurable force existing through the surface of the liquid and arising primarily from a combined effect of attractive forces between all atoms or molecules bringing them as close together as the repulsive forces arising from overlapping electron clouds will allow. For liquid metals and alloys, surface tensions arise mainly by metallic interatomic force interactions [86].

The most satisfactory and accurate methods for measuring the surface tension of liquid metals and alloys at high temperature are the sessile drop, pendant drop and drop weight method [87]. Of these three methods, only the sessile and pendant drop methods appear to be accurate over a wide range of temperatures for liquid metals and alloys. The sessile drop method was used in this study to determine the surface energies.

Laplace and Young [87] originally recognized that the attractive forces between molecules in a liquid surface create a pressure difference across a curved surface and developed equation (A-1)

$$\Delta P = \gamma_{LV}\left(\frac{1}{R_1}+\frac{1}{R_2}\right) \qquad \text{(A.1-1)}$$

where ΔP is the pressure difference between any two sides of a surface element, γ_{LV} is the surface tension and R_1 and R_2 are the principal radii of the surface.

In a sessile drop there is equilibrium between the capillary and hydrostatic pressure at some point H (Figure A.1-1) below the summit and can be mathematically expressed as

$$\Delta P = \gamma_{LV}\left(\frac{1}{R_1}+\frac{1}{R_2}\right) = g\rho_L z + P_o \qquad \text{(A.1-2)}$$

Accurate measurements of surface tension of metals and alloys can be made using a relation suggested by Dorsey [86]. The Dorsey equation is an empirical relation that depends on measurements from the top of the drop to the intersection of the axis with a 45º tangent to the drop, as shown schematically in Figure A.1-1. An advantage of this method is that it does not rely on interpolations or calculations based on tabulated parameters and is one of the accurate methods for measuring surface free energies of metals and alloys, particularly when the drop is small in diameter (1cm<diameter<4cm). In the Dorsey equation (Eq. A.1-3), f is known as the Dorsey factor, g is the gravity constant, ρ is the density of the liquid, and d_m and H' are geometrical parameters measured on the drop profile.

$$\gamma_{LV} = \frac{g\rho_L d_m^2}{4}\left(\frac{0.0520}{f} - 0.1227 + 0.0481 f\right) \quad \text{(A.1-3)}$$

$$f = \left(2H'/d_m\right) - 0.4142 \quad \text{(A.1-4)}$$

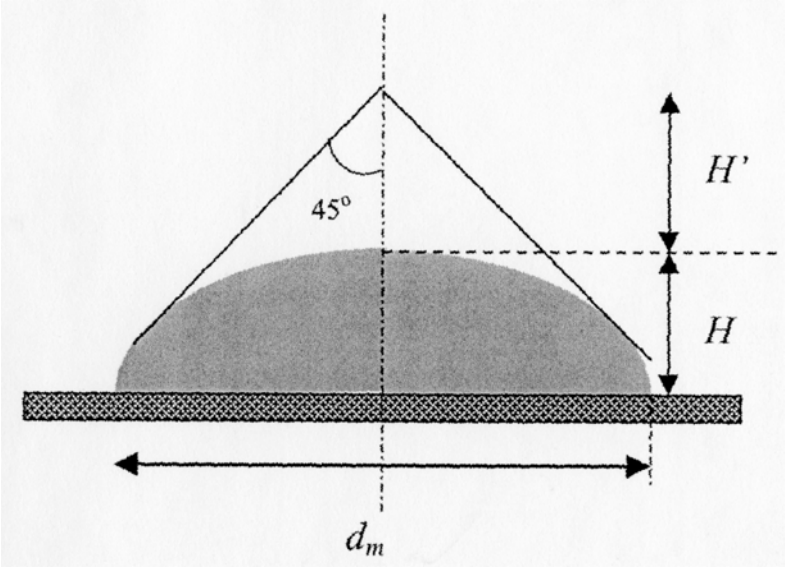

Figure A.1-1: Profile of a sessile drop and typical measurements used to calculate interfacial energy

APPENDIX B

The Alscan™ unit is based on the closed-loop gas re-circulation method. A small amount of carrier gas, usually argon, is brought in contact with the molten aluminum alloy and re-circulated through a ceramic probe that is submerged in the molten alloy, as shown in Figure A.2-1. Hydrogen diffuses into the re-circulating carrier gas until it equilibrates with the pressure of the monatomic hydrogen in the melt. At this equilibrium, and according to Sievert's law,

$$[H] \equiv S_o \sqrt{P_{H_2}} \qquad \text{(A.2-1)}$$

Where P_{H_2} is the hydrogen partial pressure over the melt, S_o is the hydrogen solubility in the alloy under 1 atm of H_2 gas (ml/100gm); and [H] is the concentration of hydrogen in the melt (ml/100gm).

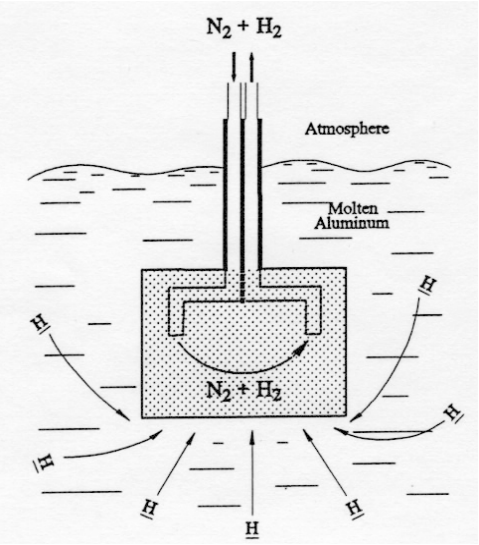

Figure A.2-1: Schematic diagram of Alscan Probe

The Alscan™ analyzer uses a “dispensable” probe that consists of a small piece of open pore ceramic in which two capillary metal tubes (the outlet and inlet for the carrier gas) are embedded. The open pore structure enhances the thermal shock resistance of the ceramic. Better thermal shock resistance obviates the need for preheating the probe. The Alscan™ analyzer is also equipped with a stirring device, which refreshes the probe/metal interface providing for a fast response time and good reproducibility. As a result, about 5 minutes are required to attain hydrogen equilibrium between the carrier gas and the metal, but a 10 minutes operation time is recommended in order to insure good reproducibility. On a hot stagnant melt, the reproducibility is typically 0.01 ml H_2 in a 100 g melt.

REFERENCES

1. Murray, J.L. and A.J. McAlister, Bulletin of Alloy Phase diagrams, 1984. **5**(1): p. 74-84.
2. Kurz, W. and D.J. Fisher, *Fundamentals of Solidification*. 1998: Trans Tech Publications.
3. Hellawell, A., Prog. Mat. Sci, 1970. **15**(3): p. 1-78.
4. Gwyer, A.G.C. and H.W.L. Phillips, J. Inst. metals., 1926. **36**: p. 283.
5. Meussner, R.A.. 1959, US Naval Res. Lab.
6. Kerr, H.W., J.A. Bell, and W.C. Winegard, J. Aust. Inst. Met.,, 1965. **10**: p. 64-69.
7. Gayler, M.L.V., J. Inst. metals., 1927. **38**: p. 157.
8. Tamman, G. and A.A. Botschwar, Z. Anorg. Chemie., 1926. **157**: p. 26.
9. Kofler, A., Z. Metallkunde, 1950. **41**: p. 22.
10. Chadwick, G., Prog. Mat. Sci, 1963. **12**(2): p. 208.
11. Davies, V.d.L. and J.M. West, J. Inst. metals., 1963-64. **92**: p. 175.
12. Scheil, E., Z. Metallkunde, 1946. **37**: p. 1.
13. Porter, D.A. and K.E. Easterling, *Phase transformations in metals and alloys*. 2nd ed. 1992: Chapman & Hall.
14. Day, M.G. and A. Hellawell, Proc. Roy. Soc. A., 1968. **305**: p. 473.
15. Major, J.F., *A Study of ultra-low growth rates of the effects of chemical additons on the solid/liquid interface of the Al/Si interface*. 1989, University of Toronto
16. Elliot, R., *Eutectic Solidification Processing*. 1983: Butterworths.

17. Rhines, F.N. and W.F.B. Timpe, Z. Metallkunde, 1957. **48**: p. 109.

18. Bell, J.A. and W.C. Winegard, J. Inst. metals., 1965. **93**: p. 318.

19. Obinata, Z. and N. Komatsu, Sci. Rep. Tohoku Univ. A, 1957. **9**: p. 107.

20. Hamilton, D.R. and R.G. Seidensticker, J.appl. phy., 1960. **31**: p. 1165-1168.

21. Billig, E. and P.J. Holmes, Acta. Cryst., 1955. **8**: p. 353.

22. Shu-zu-lu and A. Hellawell, Met. Trans., 1987. **18A**(October): p. 1721-1733.

23. Shu-zu-lu and A. Hellawell, J. Cryst. Growth, 1985. **73**: p. 316.

24. Kitamura, M., S. Hosoya, and I. Sunagawa, J. Cryst. Growth, 1979. **47**: p. 93.

25. Stranski, I.N., Disc. Faraday Soc., 1949. **5**: p. 66.

26. Sunagawa, I. and T. Yasuda, J. Cryst. Growth, 1983. **65**: p. 43.

27. Atasoy, O.A., F. Yilmaz, and R. Elliot, J. Cryst. Growth, 1984. **66**: p. 137-146.

28. Kobayashi, K. and L.M. Hogan, Phil. Mag. A, 1979. **40**(3): p. 399-407.

29. Kobayashi, K. and L.M. Hogan, J. Mat. Sci., 1985. **20**: p. 1961-1975.

30. Fredriksson, H., M. Hillert, and N. Lange, J. Inst. metals., 1973. **101**: p. 285.

31. Ino, S. and S. Ogawa, J. Phys. Soc. Japan, 1967. **22**: p. 1365.

32. Kobayashi, K. and L.M. Hogan, Metals Forum, 1978. **1**: p. 165.

33. Bernal, J.D., Nature, 1959. **183**(141).

34. Jones, B.L. and G.M. Weston, J. Mat. Sci., 1970. **5**: p. 843.

35. Lu, S. and A. Hellawell, Met. Trans., 1987. **18A**: p. 1721-1733.

36. Hanna, M.D., S.-z. lu, and A. Hellawell, Met. Trans., 1984. **15A**(March): p. 459-469.

37. Crosley, P.B. and L.F. Mondolfo, Modern Castings, 1966. **49**: p. 89-100.

38. Wamich, F. and H. Winterhager, Aluminum, 1967. **43**: p. 497.

39. Gruzleski, J.E. and B. Closset, *The Treatment of Liquid Aluminum-Silicon Alloys*. 1990, Des Plaines, Illionois: American Foundrymen's Society, Inc.

40. Mascre, C. and A. Lefebvre, Fonderie, 1959. **166**(Nov.): p. 484-499.

41. Denton, J.R. and J.A. Spittle, Mat. Sci. & Tech, 1985. **1**: p. 305-311.

42. Emadi, D., J.E. Gruzleski, and J.M. Toguri, Met. Trans.B, 1993. **24B**: p. 1055-1066.

43. Laslaz, G. and P. Laty, 1991. Birmingham, AL, USA: AFS, Des Plaines, IL, USA.

44. Fang, Q.T. and D.A. Granger, AFS Transactions, 1989. **97**: p. 989-1000.

45. Lu, S. and A. Hellawell, J. Cryst. Growth, 1985. **73**: p. 316.

46. Shamsuzzoha, M. and L.M. Hogan, Phil. Mag. A, 1986. **54**(4): p. 459-477.

47. Atasoy, O.A., Z. metallk, 1987. **78**(3): p. 177-183.

48. Shamsuzzoha, M. and L.M. Hogan, J. Cryst. Growth, 1986. **76**: p. 429-439.

49. Guillet, Rev. Mét., 1922.

50. Search, R.E., Metal Industry, 1922.

51. Curran, J.J., Chem. and Met. Engg., 1922. **27**(8): p. 860.

52. Scheil, E., Giesserei, 1959. **46**: p. 1313.

53. Patterson, W., Giesserei, 1952. **39**: p. 355.

54. Lohberg, K., Giesserei, 1957. **44**: p. 89.

55. Gurtler, G., Z. Metallkunde, 1953. **44**: p. 503.

56. Mannchen, W., Metall., 1950. **4**: p. 377.

57. Spengler, H., Metall., 1955. **9**: p. 181.

58. Tullis, D.R., J. Inst. metals., 1927. **38**: p. 181.

59. Schulz, E., Z. Metallkunde, 1949. **39**: p. 123.

60. Edwards, J.D. and R.S. Archer, Chem. and Met. Engg., 1924. **31**(13): p. 504.

61. Thall, B.M. and B. Chalmers, J. Inst. metals., 1949. **78**: p. 79.

62. Davies, V.d.L. and J.M. West, J. Inst. metals., 1963-64. **92**: p. 208.

63. Tzumara, Y., Nippon Kinzoku Gakkaisi, 1957. **21**: p. 69.

64. McLeod, A.J. and L.M. Hogan, J. Cryst. Growth, 1971. **8**: p. 61.

65. McLeod, A.J., L.M. Hogan, and C.M. Adam, J. Cryst. Growth, 1973. **19**: p. 301.

66. Clapham, L. 1987, Queens University: Kingston, Ontario, Canada

67. Mondolfo, L.F., J. Aust. Inst. Met., 1965. **10**: p. 169.

68. Bercovici, S., Private Communication, Aluminum Pechiney, France,1980.

69. Dahle, A.K. and L. Arnberg, 1994. Atlanta, GA.

70. Campbell, J., *Casting*. 1991, Oxford: Heinemann Ltd.

71. Argo, D. and J.E. Gruzleski, AFS Transactions, 1988. **96**: p. 65-74.

72. Gruzleski, J.E., et al., AFS Transactions, 1986. **94**: p. 147-154.

73. Flemings, M.C., *Solidification Processing*. 1974: New York McGraw Hill.

74. Bercovici, S., Hommes et Fonderie mars, 1979. **N-93**.

75. Dahle, A.K., J. Hjelen, and L. Arnberg, 1987. Sheffield, UK.

76. Wang, Q.G., et al., AFS Transactions, 1999.

77. Heiberg, G. and L. Arnberg, J. Light metals, 2001. **1**(1): p. 43-49.

78. Flood, S.C. and J.D. Hunt, Metal Science, 1981. **15**: p. 287.

79. Dahle, A.K., et al., Met. Trans., 2001. **32A**(4): p. 949-960.

80. Lang, G., Aluminum, 1974. **50**(11): p. 731-734.

81. Lang, G., Aluminum, 1973. **49**(3): p. 231-238.

82. Varhegyi, G., *Hungarian Patent 18, 441, Jan. 12, 1978*. 1978: Hungary.

83. Sigworth, G.K., AFS Transactions, 1983. **91**.

84. Laskowski, J.D., D. Apelian, and M.M. Makhlouf, 1996. Orlando, FL: AFS.

85. Laskowski, J.D., *Materials Science and Engineering*. 1995, Worcester Polytechnic Institute: Worcester

86. Murr, L.E., *Interfacial phenomenon in metals and alloys*. 1975, Reading, MA: Addison-Wesley Co. 87-95.

87. Liada, T. and R.I.L. Guthrie, *The Physical properties of liquid metals*. 1 ed. 1988, Oxford, England: Clarendon Press.